

Pulsed laser deposition of single phase n- and p-type Cu₂O thin films with low resistivity

Syed Farid Uddin Farhad^{1,2, 3, 4}, David Cherns¹, James Smith², Neil Fox^{1, 2}, and David Fermín³*

¹H.H. Wills Physics Laboratory, School of Physics, University of Bristol, BS8 1TL, UK

²Diamond Laboratory, School of Chemistry, University of Bristol, BS8 1TS, UK

³Electrochemistry Laboratory, School of Chemistry, University of Bristol, BS8 1TS, UK

⁴Industrial Physics Division, BCSIR Labs, Dhaka, Bangladesh Council of Scientific and Industrial Research (BCSIR), Dhaka 1205, Bangladesh

*Corresponding Author: sf1878@my.bristol.ac.uk

Abstract

Low resistivity ($\rho \sim 3\text{-}24 \text{ m}\Omega\cdot\text{cm}$) with tunable n- and p-type phase pure Cu₂O thin films have been grown by pulsed laser deposition at 25-200 °C by varying the background oxygen partial pressure (O_{2pp}). Capacitance data obtained by electrochemical impedance spectroscopy was used to determine the conductivity (n- or p-type), carrier density, and flat band potentials for samples grown on indium tin oxide (ITO) at 25 °C. The Hall mobility (μ_H) of the n- and p-type Cu₂O was estimated to be $\sim 0.85 \text{ cm}^2\cdot\text{V}^{-1}\text{s}^{-1}$ and $\sim 4.78 \text{ cm}^2\cdot\text{V}^{-1}\text{s}^{-1}$ respectively for samples grown on quartz substrate at 25 °C. An elevated substrate temperature ~ 200 °C with $O_{2pp} = 2 - 3 \text{ mTorr}$ yielded p-type Cu₂O films with six orders of magnitude higher resistivities in the range, $\rho \sim 9 - 49 \text{ k}\Omega\cdot\text{cm}$ and mobilities in the range, $\mu_H \sim 13.5 - 22.2 \text{ cm}^2\cdot\text{V}^{-1}\text{s}^{-1}$. UV-Vis-NIR diffuse reflectance spectroscopy showed optical bandgaps of Cu₂O films in the range 1.76 to 2.15 eV depending on O_{2pp} . Thin films grown at oxygen rich conditions $O_{2pp} \geq 7 \text{ mTorr}$ yielded mixed phase copper oxide irrespective of the substrate temperatures and upon air annealing at 550 °C for 1 hour completely converted to CuO phase with n-type semiconducting properties ($\rho \sim 12 \text{ }\Omega\cdot\text{cm}$, $\mu_H \sim 1.50 \text{ cm}^2 \text{ V}^{-1}\text{s}^{-1}$). The as-grown p- and n-type Cu₂O showed rectification and a photovoltaic (PV) response in solid junctions with n-ZnO and p-Si electrodes respectively. Our findings may create new opportunities for devising Cu₂O based junctions requiring low process temperatures.

1. Introduction

The semiconductor cuprous oxide (Cu_2O), has shown much promise in photocatalytic water splitting [1], resistive switching devices [2], thin film transistors (TFT) [3], gas sensors [4], as an anode material in Li-ion based batteries [5] and in photovoltaic (PV) applications [6]. It is non-toxic, Earth abundant and could be prepared by physical and chemical methods [6-8]. In addition, single phase Cu_2O is desirable as an absorber material for solar cells because of its reported optical bandgap ($E_g \sim 2.17$ eV) and high absorption coefficient (above 10^5 cm^{-1}) in the visible region of solar radiation and, potentially, the ability to dope both n- and p-type via manipulating processing conditions [9-15]. The natural p-type conductivity of Cu_2O is believed to stem from copper vacancies (V_{Cu}) in the crystal lattice [16, 17], and its suitable band alignment with other wide bandgap n-type metal oxide semiconductors, such as ZnO [18, 19] and TiO_2 [20, 21], make it much attractive for realizing reasonably efficient heterojunction solar cells. In contrast, origin of intrinsic n-type conductivity is a matter of debate [9, 22, 23], yet it has been gained substantial interest because of the possibility of the formation of homojunction solar cells [7, 9, 12, 14, 24] to suppress the deleterious interfacial defects states often formed in the case of most heterojunction solar cells ([25] and refs. therein). The oxygen vacancy (V_{O}) [11] and copper interstitial (Cu_i) defects in Cu_2O lattice have been proposed for the electron donating source in explaining the experimental results ([22] and refs. therein). In general, the donor- and acceptor- level should be shallow for good n- and p- type semiconductors respectively; and carrier concentrations over $\sim 10^{16} \text{ cm}^{-3}$ with mobility at least $\sim 5 \text{ cm}^2/\text{V.s}$ are necessary for efficient Cu_2O based optoelectronic devices [11, 26, 27]. In the case of intrinsic n-type Cu_2O , most of the experimental works reported deep donor levels ([22] and refs. therein), therefore, unlikely to overcome the native p-type conductivity stemming from cation deficiency (V_{Cu}) [6] due to the self-compensation [28].

Several physical [6, 25, 29, 30] and wet-chemical [3, 5, 15, 31-33] based deposition methods have been employed to produce phase pure Cu_2O . Among them, pulsed laser deposition (PLD) offers good control on a wide range of processing parameters such as laser wavelength, pulse repetition rate, laser energy per pulse (LP), background gas pressure ($\text{O}_{2\text{pp}}$), substrate temperature (T_{sub}) etc. and has been demonstrated to give phase pure Cu_2O with good structural, morphological and electrical properties [11, 25, 27, 34]. The ablation species reacts with ambient background gas chemically and physically while it proceeds towards the substrate from the target and affects the resulting film properties. Oxygen content in copper oxide films can be adjusted through controlling the oxygen partial pressure ($\text{O}_{2\text{pp}}$) during

growth. In the literature most of the investigations related to electrical properties of Cu-O films deal with films deposited under oxygen rich condition near the Cu₂O/CuO boundary. There is less information for films deposited at the Cu/Cu₂O boundary, where an n-type Cu₂O may exist [35] due to the predominant presence of oxygen vacancy (V_o) as opposed to the hole creating copper vacancy (V_{cu}). Meyer et al. [6], roughly estimated the binding energy of donor and acceptors for Cu₂O to be 266 meV and 156 meV using effective mass theory (EMT) and discussed that carrier density well above $\sim 10^{18} \text{ cm}^{-3}$ are necessary to overcome natural p-type conductivity due to the cation vacancy (V_{cu}). Wang et al. [36] argued that n-type conductivity of Cu₂O is possible only if the V_o would exist at very high concentrations synthesized in oxygen poor conditions. In our previous report we demonstrated the n-type conductivity of Cu₂O based on electrochemical Mott-Schottky analyses for the samples grown by PLD at room temperature with oxygen poor condition ($O_{2pp} < 1 \text{ mTorr}$)[37]. Recently, Xu et al. [11], also reported PLD grown phase pure Cu₂O films grown at 600 °C with oxygen poor condition ($O_{2pp} = 0.09 \text{ Pa} \approx 0.68 \text{ mTorr}$) with p-type conductivity and upon post N₂ plasma treatment of the as-deposited samples they observed a phase transition from pure Cu₂O to mixture of Cu₂O and Cu and a change from p to n-type conduction. Therefore, in this work, the effects of O_{2pp} (both oxygen-rich and oxygen-poor conditions) in controlling composition, microstructure structure, optical, electrical, and electrochemical impedance properties of PLD Cu₂O films were investigated. We found that under suitable deposition conditions both n- and p-type copper oxide thin films can be realized which are discussed below.

2. Experimental Procedures

2.1 Growth of PLD films

A simple PLD setup using a UV-ArF Excimer Laser (wavelength: 193 nm, repetition rate: 10Hz, pulsed width: 20 ns, spot size: $\sim 1 \text{ mm}^2$, energy(LP): $25 \pm 4 \text{ mJ/pulse}$) were used for depositing copper oxide thin films on amorphous quartz, polycrystalline ITO coated glass, and single crystalline NaCl(100) substrates under the following conditions: Base vacuum of the PLD chamber $\leq 10^{-5} \text{ Torr}$; oxygen partial pressure (O_{2pp}): 0 – 10 mTorr; target-substrate distance $\sim 5 \text{ cm}$; substrate temperature(T_{sub}): non-intentionally heated (RT $\sim 25 \text{ }^\circ\text{C}$) – 400 °C. The substrate temperature was controlled by halogen bulb heater and measured by using a digital thermocouple as described in ref.[25]. The substrate temperature and oxygen partial pressure were varied to allow the film growth in a stable regime, where no decomposition of

the film is observed. Post annealing treatment was also given to some of the as-grown Cu_2O films under controlled O_2 ambient inside the PLD chamber for comparison purpose.

Prior to film deposition, all substrates were ultrasonically cleaned successively in Toluene Acetone, isopropanol and ultra-pure water (Mili-Q, $18\text{M}\Omega\cdot\text{cm}$) for 15 min followed by a Ar blown dry. All substrates were given to a UV-Ozone cleaning for 20 min immediately before put in the PLD chamber. The target material was commercially available hot pressed ceramic Cu_2O (purity~99.95%). The target was ablated for 5 minutes prior to actual deposition on the substrates.

2.2 Characterization of PLD samples

The X-ray Diffraction (XRD) spectra were recorded with Bruker AXS D8 Advance powder X-ray diffractometer using $\text{Cu K}\alpha$ ($\lambda=1.5406 \text{ \AA}$) radiation. The diffraction patterns were recorded with a step size of $\sim 0.025^\circ$ and a time per step of 18 seconds and the samples were rotated to homogenize the measurements. TEM analyses of samples grown on $\text{NaCl}(100)$ were investigated by a JEOL 2010 and a Philips EM 430 as described in ref. [25] where TEM camera length calibration procedure was also discussed. Raman and Photoluminescence spectra were recorded at room temperature in the backscattering geometry with a Renishaw 2000 confocal spectrometer using $\lambda_{\text{ext}} = 514.5 \text{ nm}$ Ar-ion laser ($P \leq 5 \text{ mW}$) as an excitation source. The optical transmission and diffuse reflection measurements of films deposited on quartz substrate were made using a UV-VIS-NIR spectrophotometer (Shimadzu UV2600) couple with an integrating sphere. A Keithley 2400 source-measure-unit (SMU) coupled with a custom made collinear 4-point probe was used to measure sheet resistance. For highly resistive films ($>200\text{M}\Omega$) a precision current source (Keithley 6221 AC/DC) coupled with a Nanovoltmeter (Keithley 2182A) was used. To minimize the non-uniformity nature of the PLD thin film, measurement was performed at least three different areas of the sample to get a final resistance value. The thickness of the PLD films were estimated by combined analyses of FE-SEM (JEOL JSM 6330F) cross-sectional imaging and Variable Angle Spectroscopic Ellipsometry (VASE) (M-2000 U, J.A. Woollam Co.) [34]. Hall mobilities of samples grown on quartz were measured as accurately as possible using a homemade Hall coefficient measurement setup utilizing a commercial 1 Tesla permanent magnet (Magnetsales UK Ltd.) with gold coated electrical contact pads in the van der Pauw sample configuration (see supplementary materials for details). A Potentiostat (Autolab, PGSTAT-30) equipped with a frequency analyzer was used to carry

out both Cyclic Voltammetry (CV) and Electrochemical Impedance Spectroscopy (EIS) measurements under dark. An AC signal of 20 mV amplitude with frequencies ranging from 50 Hz to 10 kHz was applied at a set of constant bias voltage over a narrow potential window to preserve the stability of the Cu₂O film. The Kiethley SMU coupled with a homemade multiprobe workstation was used to measure I-V curve of the Cu₂O-based solid p-n junctions.

3. Results and discussion

Four sets of samples were grown in an attempt to grow high quality single phase copper (I) oxide (Cu₂O) at relatively low temperatures with a range of conductivities. In the first two sets of samples, substrate temperature has been varied from 25 °C(RT) to 400 °C with two different constant oxygen partial pressure(O_{2pp}), namely 3 mTorr and 10 mTorr, in order to find out the optimum process conditions for phase pure copper oxide. In other two sets, the oxygen content inside the PLD chamber has been varied ($0 \leq O_{2pp} \leq 7$ mTorr) at two substrate temperatures (T_{sub}), 25 °C and 200 °C. The PLD thin films grown at $25\text{ }^{\circ}\text{C} \leq T_{sub} \leq 400\text{ }^{\circ}\text{C}$ with constant $O_{2pp} \approx 10$ mTorr were found to be mainly composed of a mixture of Cu₂O and more O-rich Cu-O phases as evident from the XRD analyses (see Figure S1 for details). Therefore, the oxygen rich ($O_{2pp} = 10$ mTorr) samples will not be considered further in the below discussion. As a quick guide for the readers: the structural, compositional, and electrical characteristics of samples investigated are summarized in Fig. 1.

tuning the O_{2pp} allows one to achieve phase pure Cu_2O with varying electrical properties (see orange color squares and numerical value for carrier mobility in fig. 1). The structural properties of these films are presented in Fig. 2 below.

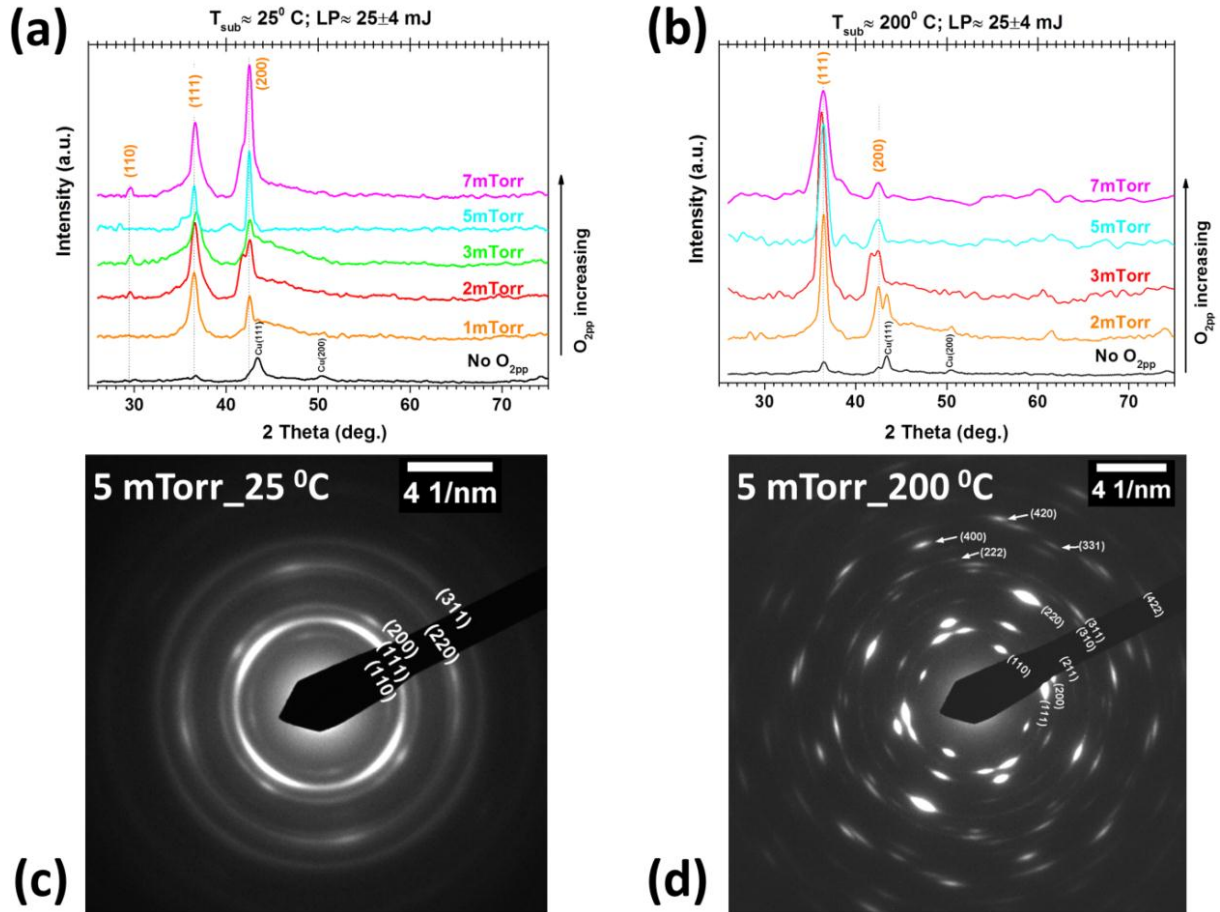


Fig. 2. (color online) PLD grown copper oxide thin films deposited at various O_{2pp} at two constant substrate temperatures: XRD patterns of Cu_2O films deposited on quartz glass at (a) $T_{sub} = 25^\circ C$ and (b) $T_{sub} = 200^\circ C$ as a function of O_{2pp} . Vertical lines (faint) represent the Bragg's reflection lines for bulk Cu_2O . SAED pattern of samples grown on $NaCl(100)$ at $T_{sub} = 25^\circ C$ (c) and $T_{sub} = 200^\circ C$ (d) with a constant $O_{2pp} = 5$ mTorr. The rings/spots are indexed to assist the reader.

Fig. 2(a) and 2(b) show the XRD profiles of as-grown films deposited at $T_{sub} = 25^\circ C$ (RT-grown) and $T_{sub} = 200^\circ C$ (HT-grown), respectively, on quartz substrate with varying O_{2pp} . XRD results revealed that single phase Cu_2O , with no contribution from Cu and CuO, could be produced with $1 \text{ mTorr} \leq O_{2pp} \leq 7 \text{ mTorr}$ in the case of RT-grown and with $3 \text{ mTorr} \leq O_{2pp} \leq 5 \text{ mTorr}$ in the case of HT-grown thin films. In these phase purity limits, both RT- and HT-grown mainly exhibit $Cu_2O(111)$ and $Cu_2O(200)$ Bragg peaks but the former

displays an additional $\text{Cu}_2\text{O}(110)$ peak at $2\theta \approx 29.5^\circ$. Metallic Cu inclusions were observed in the RT-grown film with $\text{O}_{2\text{pp}} < 1$ mTorr and in the HT-grown film with $\text{O}_{2\text{pp}} \leq 2$ mTorr presumably due to the deficiency of oxygen species in the PLD chamber. However, RT-grown film with $\text{O}_{2\text{pp}} = 1$ mTorr show phase pure Cu_2O films evident from XRD and SAED pattern (see Fig. 2(a) and Fig. 1(a)). Both RT- and HT-grown films with $\text{O}_{2\text{pp}} > 7$ mTorr were found to be mixed Cu-O phase (see figure S2) with CuO as a major product. Notice also that RT- and HT-grown films approached towards strong $\{100\}$ and $\{111\}$ texturing, respectively, with increasing $\text{O}_{2\text{pp}}$ up to 7 mTorr (see also figure S3(a)). The average crystallite domain size estimated by using Scherrer formula was found to be in the range 5 – 15 nm and found to be following a decreasing trend with increasing $\text{O}_{2\text{pp}}$ (for details see figure S3(b)) most probably due to the inclusion of oxygen rich Cu-O phase at higher $\text{O}_{2\text{pp}}$ [34]. However, up to $\text{O}_{2\text{pp}} = 5$ mTorr, PLD grown thin films are composed of Cu(I) oxide as evident from the SAED patterns shown in Fig. 2(c) and 2(d). The arced SAED patterns, more conspicuous in Fig. (d), is due to the micro-twinning on $(\bar{1}1\bar{1})$, $(1\bar{1}\bar{1})$, $(1\bar{1}1)$ and $(11\bar{1})$ planes while viewed down the $[011]$ zone axis [25] .

Room temperature Raman analyses have also been conducted to supplement the XRD results in order to further confirm the phase purity of RT-grown and at HT-grown samples deposited with $2 \text{ mTorr} \leq \text{O}_{2\text{pp}} \leq 7 \text{ mTorr}$ which are presented in Fig. 3 below. All Raman peaks in both groups of samples can be assigned with reported phonon modes of Cu_2O crystal only (solid lines) [25], except for HT-grown with $\text{O}_{2\text{pp}} = 7$ mTorr film which is seen to be a mixture of Cu_2O (solid lines) and CuO (dotted lines) (cf. Fig. 3 (a) and 3 (b)). The presence of CuO phase is confirmed by the additional presence of A_g and $B_g^{(1)}$ modes at $\sim 296 \text{ cm}^{-1}$ and $\sim 346 \text{ cm}^{-1}$ respectively (see top panel in figure 3 (b)) The position of Raman peaks for copper oxide compounds vary considerably in literature, but the vibrational modes for all three copper oxide phases cited in references [6, 25, 38] clearly indicate that none of the Raman signals in figure 3 (up to $\text{O}_{2\text{pp}} \approx 5$ mTorr in the case of HT-grown films) are related to CuO and/or Cu_4O_3 phases.

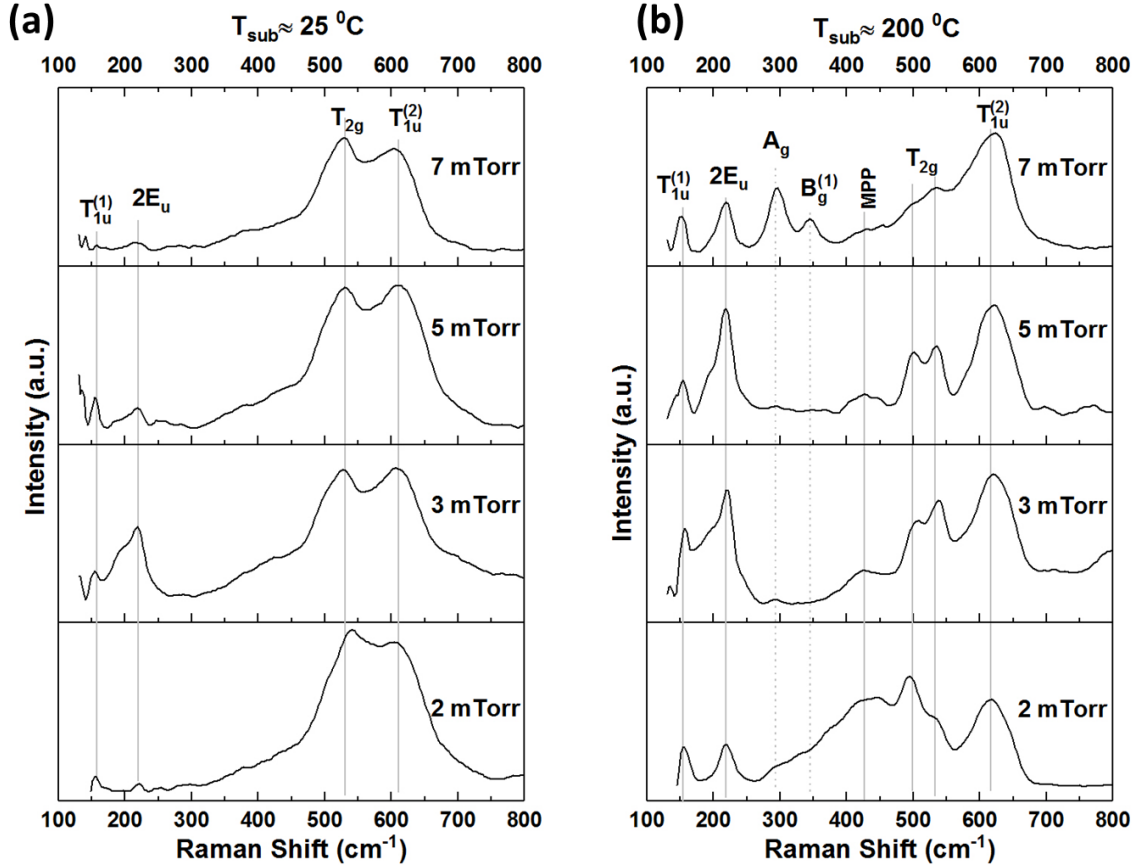


Fig. 3. Room temperature Raman spectra of, as-grown copper oxide thin films on quartz glass as a function of O_{2pp} at $T_{sub} \approx 25$ °C (a), and at $T_{sub} \approx 200$ °C (b). Vertical lines represent the reference vibrational mode of copper oxide.

The room temperature Photoluminescence (RT-PL) of thin films grown at $T_{sub} \approx 25$ °C(RT) and $T_{sub} \approx 200$ °C(HT) with $2 \text{ mTorr} \leq O_{2pp} \leq 5 \text{ mTorr}$ including Cu_2O PLD target are shown in Fig. 4. All luminescence peaks (solid lines) can be attributed to copper oxide phases, consistent with the results reported previously [25]. The exciton-related ($X_0 - \Gamma_{12}^-$) emission peak is clearly seen in the RT-PL spectrum for all PLD films including the target material suggesting good quality Cu_2O thin films irrespective of O_{2pp} conditions. The luminescence peaks centering at $\sim 760 \text{ nm}$ and $\sim 880 \text{ nm}$ have been put forward for Cu_3O_2 and $[V_{Cu}^- - V_O^+]$ complex respectively [25]. Notice that at low $O_{2pp} = 2 - 3 \text{ mTorr}$, HT-grown films showed enhanced ($X_0 - \Gamma_{12}^-$) peak with additional $[V_{Cu}^- - V_O^+]$ complex peak which is not conspicuous in RT-grown films. These samples also exhibited diminished V_{Cu} peak (see Fig. 4(b)).

The optical band gap thus approaches the bandgap value of bulk Cu_2O ($E_g = 2.17$ eV), and presumably therefore stoichiometric phase formation, at optimum values of $\text{O}_{2\text{pp}}$. The lowest measured optical bandgap (~ 1.65 eV) of HT-grown $\text{O}_{2\text{pp}} = 7$ mTorr film suggests an oxygen rich Cu-O phase as also evident from its Raman spectrum (see top panel in Fig. 3(b)). The RT-grown sample (S1) annealed in air at 550°C for 1 hour also exhibited a lower optical bandgap ~ 1.45 eV due to complete conversion to CuO (see figure S4 in supplemental materials). The lower optical bandgap for films with low $\text{O}_{2\text{pp}}$, suggest oxygen vacancies (V_o) which introduce defect states in the bandgap leading to a lower effective bandgap compared to the stoichiometric Cu_2O .

Fig. 6 (below) shows the four point collinear probe measured electrical resistivity of RT- and HT-grown films as a function of $\text{O}_{2\text{pp}}$. The data points for the films grown without O_2 injection in the PLD chamber have also been included in the analyses for the sake of completeness and comparison.

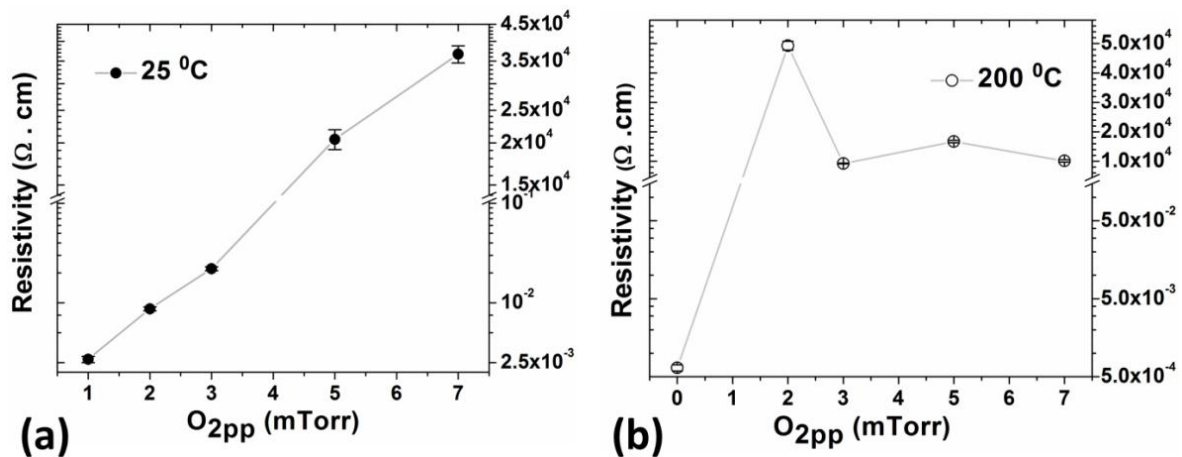


Fig. 6. Variation of Electrical resistivity of as-grown copper oxide thin films onto quartz glass as a function of $\text{O}_{2\text{pp}}$ deposited at $T_{\text{sub}} \approx 25^\circ\text{C}$ (a) and $T_{\text{sub}} \approx 200^\circ\text{C}$ (b).

As can be seen from the Fig. 6(a), the resistivities of RT-grown films are found to be monotonically increasing with increasing $\text{O}_{2\text{pp}}$. At $1 \text{ mTorr} \leq \text{O}_{2\text{pp}} \leq 3 \text{ mTorr}$ PLD ambient their resistivities were estimated to be roughly $3 - 24 \text{ m}\Omega \cdot \text{cm}$ which is ~ 3 orders of magnitude lower than the reported resistivity ($40 - 60 \Omega \cdot \text{cm}$) for Cu_2O films grown by PLD above $T_{\text{sub}} \geq 600^\circ\text{C}$ [40]. On the other hand, the resistivities of RT-films with $5 \text{ mTorr} \leq \text{O}_{2\text{pp}} \leq 7 \text{ mTorr}$ PLD ambient are quite high, roughly in the range $20 - 38 \text{ k}\Omega \cdot \text{cm}$ (see Fig. 6(a)) due to more stoichiometric Cu_2O phase formed in the oxygen rich conditions. In contrast, the resistivity of HT-grown film without injecting O_2 into the PLD chamber was

estimated to be below 7 mΩ.cm (see Fig. 6(b)). The HT-grown film deposited using $O_{2pp} = 2$ mTorr exhibited the highest resistivity of ~49 kΩ.cm among all samples, probably due to inclusion of metallic Cu into the Cu_2O matrix which compensates available holes leading to insulating thin films [26]. The resistivities of $2 \text{ mTorr} \leq O_{2pp} \leq 7 \text{ mTorr}$ HT-grown films are roughly six orders of magnitude higher than that of the film grown without oxygen. These results are also suggesting that oxygen rich PLD ambient leads to more stoichiometric copper oxide, thereby resulting in more insulating thin films due to the lack of charge carrier creating defect (vacancy type) concentrations.

Hall coefficient measurements and Mott-Schottky plots (see Fig. 7(a)) constructed from electrochemical impedance spectra [9, 31] were also carried out for samples grown with identical deposition PLD conditions on quartz and ITO substrates respectively (see figure S7 on supplementary material)). The results together with optical bandgap values are summarized in Table 1. As can be seen, samples grown with $O_{2pp} = 2 - 3$ mTorr, showed a p-type conductivity with appreciable Hall mobility (μ_H)~ $4.78 \pm 0.01 \text{ cm}^2 \text{ V}^{-1} \text{ s}^{-1}$ and $\sim 22.20 \pm 0.01 \text{ cm}^2 \text{ V}^{-1} \text{ s}^{-1}$ respectively in RT- and HT-grown PLD Cu_2O films. The higher mobility in HT-grown PLD films could be attributed to the better crystalline and optoelectronic quality evident from XRD, SAED, Raman, and RT-PL analyses. However, the lower carrier concentrations ($\sim 6 \times 10^{12-13} \text{ cm}^{-3}$) of HT-grown films may be attributed to the hole killing $[V_{Cu}^- - V_O^+]$ defect complex seen in PL spectra (see Fig. 4(b)).

Table 1

Optical and Electrical properties of phase pure Cu₂O and CuO thin films deposited with low O_{2pp} content during growth.

Growth condition (T _{sub} _O _{2pp})	Band gap (eV) ± 0.01	Thickness (nm) (VASE/ SEM)	Resistivity (Ω.cm)	Carrier density (cm ⁻³) [Hall effect meas.]	Hall Mobility (cm ² /V.s) ± 0.01	Carrier density (cm ⁻³) [EIS meas.]
25_1	1.76	556±21	2.12×10 ⁻³	-3.47×10 ²¹	0.85	-(1.24±.03)×10 ²¹
25_2	1.80	562±4	8.71×10 ⁻³	6.97×10 ²⁰	1.03	-
25_3	2.00	615±25	24.00×10 ⁻³	5.45×10 ¹⁹	4.78	(1.39±.01)×10 ²⁰
200_2	1.90	510±7	49.28×10 ³	5.71×10 ¹²	22.21	-
200_3	2.00	585±7	9.25×10 ³	5.02×10 ¹³	13.45	-
Ann. S1(CuO)	1.50	Assumed ~500	12.2 ± 7	-3.42×10 ¹⁷	1.50	-

The acceptor concentration, $N_a \sim 6 \times 10^{12-13} \text{ cm}^{-3}$ and mobility, $\mu_H \sim 13-22 \text{ cm}^2 \text{ V}^{-1} \text{ s}^{-1}$ estimated for T_{sub} ≈ 200 °C(HT) samples are consistent with previous results [6]. The high mobility indicates that PLD films grown at 200 °C possess reasonably good electrical quality, however, a carrier concentration as high as $\sim 10^{14} - 10^{16} \text{ cm}^{-3}$ is desirable for potential Cu₂O based device applications [27]. Therefore, for some specific device applications [3, 26, 41] RT-grown PLD Cu₂O may be utilized.

Notice that carrier density in RT-grown samples is exceptionally high compared to that of HT-grown samples. For example, with O_{2pp} = 2 mTorr, carrier density $\sim (5.71 \pm 0.18) \times 10^{12} \text{ cm}^{-3}$ estimated for HT-grown sample is at least eight order of magnitude lower than the carrier density $\sim (6.97 \pm 0.01) \times 10^{20} \text{ cm}^{-3}$ for RT-grown samples. With increasing O_{2pp} content slightly to 3 mTorr for RT-grown sample, it was estimated as $\sim (5.45 \pm 0.23) \times 10^{19} \text{ cm}^{-3}$ which is still roughly six order magnitude higher compared to its HT-grown counterpart.

The effective density of states ($D(E_f)$) for these samples are in the range ($D(E_f)$) $\sim 1.35 - 5.67 \times 10^{21} \text{ (eV)}^{-1} \text{ cm}^{-3}$ estimated from EIS data by a similar approach presented in ref. [42] using the equation : $D(E_f) = (C_{sc})^2 / [\epsilon_0 \epsilon. e^2]$, where, C_{sc} is the space charge capacitance, ϵ_0 is permittivity of free space ($8.854 \times 10^{-12} \text{ F.m}^{-1}$), ϵ is the relative dielectric constant (~ 6.6 for Cu_2O [31]) and e is the electronic charge (see supplemental material for detail calculations). The high level of N_a , is consistent with low resistivity (few $\text{m}\Omega.\text{cm}$), and low Hall mobilities (μ_H) $\sim 1.03 - 4.78 \text{ cm}^2\text{V}^{-1}\text{s}^{-1}$ could be attributed to the scattering of holes at the grain boundaries of these RT-grown nanocrystalline films.

In contrast, the samples grown at $1 \text{ mTorr}_- 25^\circ\text{C(RT)}$ exhibited an n-type conductivity with high level of donor concentrations (N_d) $\sim 3.47 \times 10^{21} \text{ cm}^{-3}$ ($\mu_H \sim 0.85 \pm 0.01 \text{ cm}^2 \text{ V}^{-1}\text{s}^{-1}$) and $\sim 1.24 \times 10^{21} \text{ cm}^{-3}$ estimated from Hall coefficient measurement and M-S analyses respectively. The effective density of states ($D(E_f)$) for this sample is $1.05 \times 10^{20} \text{ (eV)}^{-1} \text{ cm}^{-3}$ slightly lower compared to p-type RT-grown samples. However, such high level of carrier concentrations may contribute to its exceptionally low resistivity of $\sim 3 \text{ m}\Omega.\text{cm}$. The optical bandgap ($\sim 1.76 \text{ eV}$) of this n-type sample suggest that donor level may be shallow. In literature, the Fermi level of donor and acceptor levels for intrinsic Cu_2O is rarely reported ([9],[22] and refs. therein). An approximate band diagram of PLD-grown Cu_2O thin film electrode is shown in Fig. 7(b) using electrochemical M-S plot and UV-VIS-NIR optical data to demonstrate the quasi Fermi level energy of E_f^e ($\sim 0.28 \text{ eV}$ below CBM) and E_f^h ($\sim 0.13 \text{ eV}$ above VBM) for donor and acceptor states respectively. The Fermi level is estimated from Flat band potentials -0.72 V vs RHE (Fermi energy with respect to vacuum, $E_f = -3.73 \text{ eV}$) and $+0.91 \text{ V vs RHE}$ ($E_f = -5.37 \text{ eV}$) respectively for n- and p-type $\text{Cu}_2\text{O/ITO}$ electrodes using similar approach described in ref. [9]. The distinct positive- and negative- slope seen in M-S plots in Fig. 7(a) confirms the n- and p-type conductivity of $\text{Cu}_2\text{O/ITO}$ electrodes and as seen in Fig. 7(b) the donor level is obviously located in more positive potentials than the acceptor level for Cu_2O which corroborate the reported results [9, 24] . The estimated E_f^e $\sim 0.28 \text{ eV}$ below the conduction band minimum (CBM) considerably shallower than the results of Garuthara et al. ($\sim 0.38 \text{ eV}$) [43] and E_f^h $\sim 0.13 \text{ eV}$ above the valence band maximum (VBM) which is little small compared to $\sim 0.22 \text{ eV}$ for V_{cu} and $\sim 0.47 \text{ eV}$ for $V_{\text{cu,split}}$ [22] .

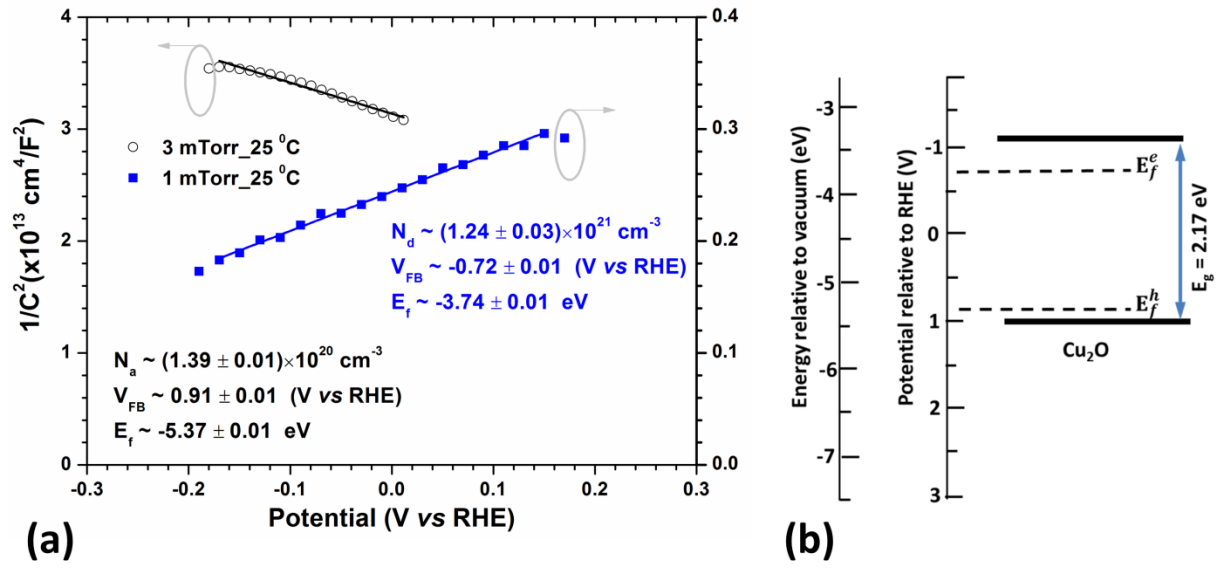


Fig. 7. (a) Mott-Schottky plots of Cu₂O thin films grown on ITO using 1 mTorr_25 °C and 3 mTorr_25 °C deposition conditions showing n-type and p-type conductivity respectively. The estimated carrier concentration, Flat band potential (V_{FB}) and quasi Fermi level energy (E_f^x ; where $x = e$ or h) for donor and acceptor states are also shown in the inset. (b) An approximate band diagram of Cu₂O grown at low O_{2pp} and T_{sub} by PLD.

The low resistivity ($\rho \sim 3 \text{ m}\Omega \cdot \text{cm}$) of n-type PLD grown Cu₂O films is yet at least ~ 3 order of magnitude above the resistivity of thermally evaporated metallic Cu ($3.5 \text{ }\mu\Omega \cdot \text{cm}$) and Cu+Cu₂O ($27 \text{ }\mu\Omega \cdot \text{cm}$) thin films reported by Figueiredo et al. [29]. Additionally, samples grown at 1 mTorr_25 °C (RT) are single phase Cu₂O evident from both XRD (Fig. 2(a)) and TEM (Fig. 1(a)) analyses and they are the most oxygen deficient phase pure Cu₂O among the samples deposited in this study. Therefore, the origin of n-type conductivity in these PLD films is presumably due to the electron generating predominant oxygen vacancy (V_o) at the vicinity of Cu/Cu₂O phase boundary [23, 35]. The phase pure n-type Cu₂O deposited by electrodeposition with N_d as high as $\sim 10^{20} \text{ cm}^{-3}$ [15] is repeatedly appear in literatures, but phase pure n-type Cu₂O deposited by PLD is rarely reported. Recently, Xu et al. [11] reported PLD grown phase pure Cu₂O using $O_{2pp} = 0.09 \text{ Pa}$ at $T_{sub} = 600 \text{ }^\circ\text{C}$ with p-type conductivity and they were able to convert them into n-type Cu₂O via post-deposition N₂ plasma treatment. However, in our study the slight increase of O_{2pp} from 1 to 2 mTorr or more in the PLD chamber yielded p-type Cu₂O films suggesting that n-type Cu₂O can only be stabilized in a narrow range of $O_{2pp} \leq 1 \text{ mTorr}$. Our findings for RT-grown samples suggest that critical regulation of low level O_{2pp} help achieving phase pure Cu₂O with tunable optical band gap ($E_g = 1.76 - 2.15 \text{ eV}$) and type of conductivity with appreciable hall mobilities ($\mu_H \sim 0.85 -$

4.78 cm² V⁻¹s⁻¹). Compared to results reported by Xu et al. this is important for synthesizing diverse optoelectronic device with low thermal budget [3, 41] including p-n Cu₂O based homojunctions [7, 9, 12, 14, 24].

It is conspicuous that estimated acceptor concentrations in RT-grown p-Type Cu₂O samples are also high ($N_a \sim 6 \times 10^{19-20}$ cm⁻³) in our observations (see Table 1 and Fig. 7). This is consistent with other recent reports. Theoretical studies reported by Raebiger et al. [16] suggest that the dominant defect V_{Cu} can be even above 10²¹ cm⁻³ in concentrations, both in Cu-rich(oxygen poor) and Cu-poor(oxygen rich) growth conditions, to produce a p-type conductivity. Recent experimental works conducted by Zhang et al. [44] reported hole concentrations in the range $5.81 \times 10^{18} - 2.17 \times 10^{21}$ cm⁻³ for sputtered Cu₂O thin films grown at room temperatures. Chen et al. [45] also reported that hole concentrations could be as high as 1.5×10^{21} cm⁻³.

The PLD sample (S1) annealed at 550 °C in air for 1 hour is phase pure CuO and showed n-type conductivity with carrier concentration $\sim 3.47 \times 10^{17}$ cm⁻³ and mobility ~ 1.5 cm² V⁻¹s⁻¹ consistent with reported result [30]. The n-type conductivity of CuO can be understood as follows. PLD grown Cu₂O thin films with high O_{2pp} are copper deficient p-type semiconductors where the type of conductivity arises from the copper vacancies can be described by following equation:



where, O_O - oxygen in regular positions of the lattice, V_{Cu}⁻ - metal vacancies, and h⁺ - holes. Due to annealing of p-type Cu₂O in air, more and more oxygen species are escaped from the Cu₂O matrix and generate more Cu²⁺ at the expense of Cu¹⁺ in the films (and recrystallizes to CuO phase) leading to the creation of electron-generating oxygen vacancy (V_O⁺²) according to the following equation:



where, V_O⁺² - oxygen vacancies, and e⁻ - electrons. As seen from the equation (2), evolution of oxygen is accompanied by the formation of oxygen vacancies (with effective positive charge) and electrons that determine n-type of conductivity.

As a proof-of-concept, solid p-n junctions were fabricated with FTO/n-ZnO/p-Cu₂O/Au and p-Si(111)/n-Cu₂O structures. Their stable current-voltage characteristic curves

suggest that p-n junctions were formed successfully, albeit with poor photovoltaic performance. These results are summarized and discussed in the supplementary materials (see figures S12 - S14).

4. Conclusions

Phase pure n- and p-type Cu_2O thin films were grown on quartz glass and other substrates (ITO, $\text{NaCl}(100)$, and $\text{p-Si}(111)$) by PLD technique and the influence of substrate temperatures and oxygen pressure ($\text{O}_{2\text{pp}}$) on the films properties were explored systematically. Thin films grown at $25^\circ\text{C}(\text{RT})$ and $200^\circ\text{C}(\text{HT})$ substrate temperatures are single phase Cu_2O with (200) and (111) texture respectively and their texturing found to be increasing with the increasing oxygen content in the $2\text{ mTorr} \leq \text{O}_{2\text{pp}} \leq 5\text{ mTorr}$ PLD ambient. The optical bandgaps and electrical resistivities of RT-grown Cu_2O thin films were found to be tunable in the range $1.76\text{ eV} - 2.15\text{ eV}$ and $3\text{ m}\Omega.\text{cm} - 38\text{ k}\Omega.\text{cm}$ respectively and both properties were found to be consistently increasing from low to higher values with increasing $\text{O}_{2\text{pp}}$ due to more stoichiometric Cu(I) phase formation. Critical regulations of low level $\text{O}_{2\text{pp}}$ during process help achieving both n- and p-type Cu_2O with appreciable hall mobilities ($\mu_{\text{H}} \sim 0.85 - 4.78\text{ cm}^2\text{ V}^{-1}\text{ s}^{-1}$). The as-grown phase pure p- and n-type Cu_2O showed promising rectification in solid junctions with n-ZnO and p-Si electrodes respectively. Our findings suggest that critical regulations of PLD growth conditions help achieving single phase Cu_2O with tunable physical properties desirable for diverse optoelectronic applications.

Acknowledgments

S.F.U. Farhad acknowledges the financial help through BANGABANDHU fellowship, Ministry of Science and Technology, Government of Bangladesh to conduct this research. The authors are indebted to Professor Mike Ashfold FRS for allowing his PLD setup located at Diamond laboratory, School of Chemistry, University of Bristol, UK during the Ph.D. studies. Special thanks are also due to Professor Walther Schawrzner, School of Physics, University of Bristol, UK for lending his Kiethley SMU2400 instrument in building a custom-made 4-point collinear probe resistivity measurement setup. S.F.U Farhad also acknowledges the PV characterization support of the Energy Conversion and Storage Research (ECSR) section, Industrial Physics Division, BCSIR Labs, Dhaka, Bangladesh.

Conflict of interest: We declare that we have no conflict of interest.

Author Contributions: S.F.U. Farhad and D.Cherns conceived the idea and S.F.U. Farhad did the experimental works and wrote the manuscript. J.Smith and N. Fox helped with the deposition setup and Hall coefficient measurements. D. Fermin helped with electrochemical measurements and analyses. All authors contributed in editing and reviewing of the final manuscript.

References

- [1] H. Kim, S. Bae, D. Jeon, J. Ryu, Fully solution-processable Cu_2O – BiVO_4 photoelectrochemical cells for bias-free solar water splitting, *Green Chemistry*, 20 (2018) 3732-3742.
- [2] Y.S. Zhi, P.G. Li, P.C. Wang, D.Y. Guo, Y.H. An, Z.P. Wu, X.L. Chu, J.Q. Shen, W.H. Tang, C.R. Li, Reversible transition between bipolar and unipolar resistive switching in $\text{Cu}_2\text{O}/\text{Ga}_2\text{O}_3$ binary oxide stacked layer, *AIP Advances*, 6 (2016) 015215.
- [3] D. Muñoz-Rojas, M. Jordan, C. Yeoh, A.T. Marin, A. Kursumovic, L.A. Dunlop, D.C. Iza, A. Chen, H. Wang, J.L. MacManus Driscoll, Growth of $\sim 5 \text{ cm}^2\text{V}^{-1}\text{s}^{-1}$ mobility, p-type Copper(I) oxide (Cu_2O) films by fast atmospheric atomic layer deposition (AALD) at 225°C and below, *AIP Advances*, 2 (2012) 042179.
- [4] H. Zhang, Q. Zhu, Y. Zhang, Y. Wang, L. Zhao, B. Yu, One-Pot Synthesis and Hierarchical Assembly of Hollow Cu_2O Microspheres with Nanocrystals-Composed Porous Multishell and Their Gas-Sensing Properties, *Advanced Functional Materials*, 17 (2007) 2766-2771.
- [5] K. Chen, S. Song, D. Xue, Faceted Cu_2O structures with enhanced Li-ion battery anode performances, *CrystEngComm*, 17 (2015) 2110-2117.
- [6] B.K. Meyer, A. Polity, D. Reppin, M. Becker, P. Hering, P.J. Klar, T. Sander, C. Reindl, J. Benz, M. Eickhoff, C. Heiliger, M. Heinemann, J. Bläsing, A. Krost, S. Shokovets, C. Müller, C. Ronning, Binary copper oxide semiconductors: From materials towards devices, *physica status solidi (b)*, 249 (2012) 1487-1509.
- [7] L.C. Olsen, F.W. Addis, W. Miller, Experimental and theoretical studies of Cu_2O solar cells, *Solar Cells*, 7 (1982) 247-279.
- [8] A.E. Rakhshani, Preparation, characteristics and photovoltaic properties of cuprous oxide—a review, *Solid-State Electronics*, 29 (1986) 7-17.
- [9] C.M. McShane, K.S. Choi, Junction studies on electrochemically fabricated p-n Cu_2O homojunction solar cells for efficiency enhancement, *Physical chemistry chemical physics : PCCP*, 14 (2012) 6112-6118.
- [10] L. Xiong, S. Huang, X. Yang, M. Qiu, Z. Chen, Y. Yu, p-Type and n-type Cu_2O semiconductor thin films: Controllable preparation by simple solvothermal method and photoelectrochemical properties, *Electrochimica Acta*, 56 (2011) 2735-2739.
- [11] M. Xu, X. Liu, W. Xu, H. Xu, X. Hao, X. Feng, Low resistivity phase-pure n-type Cu_2O films realized via post-deposition nitrogen plasma treatment, *Journal of Alloys and Compounds*, 769 (2018) 484-489.
- [12] R.P. Wijesundera, L.K.A.D.D.S. Gunawardhana, W. Siripala, Electrodeposited Cu_2O homojunction solar cells: Fabrication of a cell of high short circuit photocurrent, *Solar Energy Materials and Solar Cells*, 157 (2016) 881-886.
- [13] J. Han, J. Chang, R. Wei, X. Ning, J. Li, Z. Li, H. Guo, Y. Yang, Mechanistic investigation on tuning the conductivity type of cuprous oxide (Cu_2O) thin films via deposition potential, *International Journal of Hydrogen Energy*, 43 (2018) 13764-13777.

- [14] K. Han, M. Tao, Electrochemically deposited p–n homojunction cuprous oxide solar cells, *Solar Energy Materials and Solar Cells*, 93 (2009) 153-157.
- [15] P. Wang, H. Wu, Y. Tang, R. Amal, Y.H. Ng, Electrodeposited Cu_2O as Photoelectrodes with Controllable Conductivity Type for Solar Energy Conversion, *The Journal of Physical Chemistry C*, 119 (2015) 26275-26282.
- [16] H. Raebiger, S. Lany, A. Zunger, Origins of the p-type nature and cation deficiency in Cu_2O and related materials, *Physical Review B*, 76 (2007).
- [17] L.Y. Isseroff, E.A. Carter, Electronic Structure of Pure and Doped Cuprous Oxide with Copper Vacancies: Suppression of Trap States, *Chemistry of Materials*, 25 (2013) 253-265.
- [18] K.P. Musselman, A. Marin, A. Wisnet, C. Scheu, J.L. MacManus-Driscoll, L. Schmidt-Mende, A Novel Buffering Technique for Aqueous Processing of Zinc Oxide Nanostructures and Interfaces, and Corresponding Improvement of Electrodeposited $\text{ZnO-Cu}_2\text{O}$ Photovoltaics, *Advanced Functional Materials*, 21 (2011) 573-582.
- [19] S.S. Wilson, J.P. Bosco, Y. Tolstova, D.O. Scanlon, G.W. Watson, H.A. Atwater, Interface stoichiometry control to improve device voltage and modify band alignment in $\text{ZnO/Cu}_2\text{O}$ heterojunction solar cells, *Energy Environ. Sci.*, 7 (2014) 3606-3610.
- [20] M. Pavan, S. Rühle, A. Ginsburg, D.A. Keller, H.-N. Barad, P.M. Sberna, D. Nunes, R. Martins, A.Y. Anderson, A. Zaban, E. Fortunato, $\text{TiO}_2/\text{Cu}_2\text{O}$ all-oxide heterojunction solar cells produced by spray pyrolysis, *Solar Energy Materials and Solar Cells*, 132 (2015) 549-556.
- [21] K. Kardarian, D. Nunes, P. Maria Sberna, A. Ginsburg, D.A. Keller, J. Vaz Pinto, J. Deuermeier, A.Y. Anderson, A. Zaban, R. Martins, E. Fortunato, Effect of Mg doping on Cu_2O thin films and their behavior on the $\text{TiO}_2/\text{Cu}_2\text{O}$ heterojunction solar cells, *Solar Energy Materials and Solar Cells*, 147 (2016) 27-36.
- [22] D.O. Scanlon, G.W. Watson, Undoped n-Type Cu_2O : Fact or Fiction?, *The Journal of Physical Chemistry Letters*, 1 (2010) 2582-2585.
- [23] L. Frazer, K.B. Chang, R.D. Schaller, K.R. Poeppelmeier, J.B. Ketterson, Vacancy relaxation in cuprous oxide ($\text{Cu}_{2-x}\text{O}_{1-y}$), *Journal of Luminescence*, 183 (2017) 281-290.
- [24] L.C.-K. Liao, Y.-C. Lin, Y.-J. Peng, Fabrication Pathways of p–n Cu_2O Homojunction Films by Electrochemical Deposition Processing, *The Journal of Physical Chemistry C*, 117 (2013) 26426-26431.
- [25] S.F.U. Farhad, R.F. Webster, D. Cherns, Electron microscopy and diffraction studies of pulsed laser deposited cuprous oxide thin films grown at low substrate temperatures, *Materialia*, 3 (2018) 230 - 238.
- [26] X. Liu, M. Xu, X. Zhang, W. Wang, X. Feng, A. Song, Pulsed-laser-deposited, single-crystalline Cu_2O films with low resistivity achieved through manipulating the oxygen pressure, *Applied Surface Science*, 435 (2018) 305-311.
- [27] S.H. Wee, P.S. Huang, J.K. Lee, A. Goyal, Heteroepitaxial Cu_2O thin film solar cell on metallic substrates, *Scientific reports*, 5 (2015) 16272.
- [28] S. Ishizuka, K. Akimoto, Control of the growth orientation and electrical properties of polycrystalline Cu_2O thin films by group-IV elements doping, *Applied Physics Letters*, 85 (2004) 4920.
- [29] V. Figueiredo, E. Elangovan, G. Gonçalves, P. Barquinha, L. Pereira, N. Franco, E. Alves, R. Martins, E. Fortunato, Effect of post-annealing on the properties of copper oxide thin films obtained from the oxidation of evaporated metallic copper, *Applied Surface Science*, 254 (2008) 3949-3954.
- [30] X. Hu, F. Gao, Y. Xiang, H. Wu, X. Zheng, J. Jiang, J. Li, H. Yang, S. Liu, Influence of oxygen pressure on the structural and electrical properties of CuO thin films prepared by pulsed laser deposition, *Materials Letters*, 176 (2016) 282-284.
- [31] A. Paracchino, J.C. Brauer, J.-E. Moser, E. Thimsen, M. Graetzel, Synthesis and Characterization of High-Photoactivity Electrodeposited Cu_2O Solar Absorber by Photoelectrochemistry and Ultrafast Spectroscopy, *The Journal of Physical Chemistry C*, 116 (2012) 7341-7350.

- [32] S.F.U. Farhad, M.A. Hossain, N.I. Tanvir, R. Akter, M.A.M. Patwary, M. Shahjahan, M.A. Rahman, Structural, optical, electrical, and photoelectrochemical properties of cuprous oxide thin films grown by modified SILAR method, *Materials Science in Semiconductor Processing*, 95 (2019) 68-75.
- [33] Y. Yang, J. Han, X. Ning, W. Cao, W. Xu, L. Guo, Controllable morphology and conductivity of electrodeposited Cu_2O thin film: effect of surfactants, *ACS Appl Mater Interfaces*, 6 (2014) 22534-22543.
- [34] S.F.U. Farhad, Copper Oxide Thin Films grown by Pulsed Laser Deposition for Photovoltaic Applications, in: *School of Physics, University of Bristol, UK, British Library EThOS*, January 2016, pp. 222.
- [35] O. Porat, I. Riess, Defect chemistry of Cu_{2-y}O at elevated temperatures.
- Part II: Electrical conductivity, thermoelectric power and charged point defects, *Solid State Ionics*, 81 (1995).
- [36] Y. Wang, P. Miska, D. Pilloud, D. Horwat, F. Mücklich, J.F. Pierson, Transmittance enhancement and optical band gap widening of Cu_2O thin films after air annealing, *Journal of Applied Physics*, 115 (2014) 073505.
- [37] S.F.U. Farhad, D. Cherns, Structural, Optical and Electrical properties of nanocrystalline Cu_2O thin films grown by Pulsed Laser Deposition, in: *2014 MRS Spring Meeting and Exhibition, Material Research Society(MRS), San Francisco, California, USA., 2014.*
- [38] L. Debbichi, M.C. Marco de Lucas, J.F. Pierson, P. Krüger, Vibrational Properties of CuO and Cu_4O_3 from First-Principles Calculations, and Raman and Infrared Spectroscopy, *The Journal of Physical Chemistry C*, 116 (2012) 10232-10237.
- [39] S.F.U. Farhad, N.I. Tanvir, M.S. Bashar, M.S. Hossain, M. Sultana, N. Khatun, Facile synthesis of oriented zinc oxide seed layer for the hydrothermal growth of zinc oxide nanorods, *Bangladesh Journal of Scientific and Industrial Research*, 53 (2018) 233.
- [40] S.B. Ogale, P.G. Bilurkar, N. Mate, S.M. Kanetkar, N. Parikh, B. Patnaik, Deposition of copper oxide thin films on different substrates by pulsed excimer laser ablation, *Journal of Applied Physics*, 72 (1992) 3765-3769.
- [41] A. Subramaniyan, J.D. Perkins, R.P. O'Hayre, S. Lany, V. Stevanovic, D.S. Ginley, A. Zakutayev, Non-equilibrium deposition of phase pure Cu_2O thin films at reduced growth temperature, *APL Materials*, 2 (2014) 022105.
- [42] B. Bera, A. Chakraborty, T. Kar, P. Leuaa, M. Neergat, Density of States, Carrier Concentration, and Flat Band Potential Derived from Electrochemical Impedance Measurements of N-Doped Carbon and Their Influence on Electrocatalysis of Oxygen Reduction Reaction, *The Journal of Physical Chemistry C*, 121 (2017) 20850-20856.
- [43] R. Garuthara, W. Siripala, Photoluminescence characterization of polycrystalline n-type Cu_2O films, *Journal of Luminescence*, 121 (2006) 173-178.
- [44] L. Zhang, L. McMillon, J. McNatt, Gas-dependent bandgap and electrical conductivity of Cu_2O thin films, *Solar Energy Materials and Solar Cells*, 108 (2013) 230-234.
- [45] X. Chen, D. Parker, M.-H. Du, D.J. Singh, Potential thermoelectric performance of hole-doped Cu_2O , *New Journal of Physics*, 15 (2013) 043029.

Supporting information

Pulsed laser deposition of single phase n- and p-type Cu₂O thin films with low resistivity

Syed Farid Uddin Farhad^{1,2, 3, 4}, David Cherns¹, James Smith², Neil Fox^{1, 2}, and David Fermín³*

¹H.H. Wills Physics Laboratory, School of Physics, University of Bristol, BS8 1TL, UK

²Diamond Laboratory, School of Chemistry, University of Bristol, BS8 1TS, UK

³Electrochemistry Laboratory, School of Chemistry, University of Bristol, BS8 1TS, UK

⁴Industrial Physics Division, BCSIR Labs, Dhaka, Bangladesh Council of Scientific and Industrial Research (BCSIR), Dhaka 1205, Bangladesh

*Corresponding Author: sf1878@my.bristol.ac.uk

Copper oxide films grown with O_{2pp} = 10 mTorr at T_{sub} = 25 - 400 °C :

As evident from Figure S1 (a) below, thin films deposited up to T_{sub} ≈ 100 °C, show a mixture of CuO and Cu₂O phases with no specific orientation. For the films grown at T_{sub} ≥ 200 °C, the XRD patterns show no clear evidence of CuO and Cu₄O₃ phases (see the respective ICSD patterns given in the figure), but strong Cu₂O(111) and Cu₂O(200) reflection peaks. There is also evidence for some metallic Cu with (111) and (200) planes visible at T_{sub} ≥ 300 °C. In addition, Cu₂O phase is seen to be increasing with the expense of CuO phase, suggesting that an elevated temperature might be more favourable for PLD ablated adatoms to form phase pure Cu₂O but it also suggests that even O_{2pp} = 10 mTorr is not enough to suppress Cu within 300 °C ≤ T_{sub} ≤ 400 °C regime (see blue and orange curve in Figure S1). The likely reason of the absence of CuO but the presence of Cu₂O and Cu most probably due to the dissolving of O species from the Cu-O films in 300 °C ≤ T_{sub} ≤ 400 °C regime. However, presence of Cu in oxygen rich films at T_{sub} ≥ 300 °C is quite unexpected, as the reduction of the Cu₂O directly to Cu, particularly in absence of any reducing agent, is thermodynamically unfavourable. These results suggest that scope of controlling the phase purity is less certain in case of oxygen rich PLD ambient.

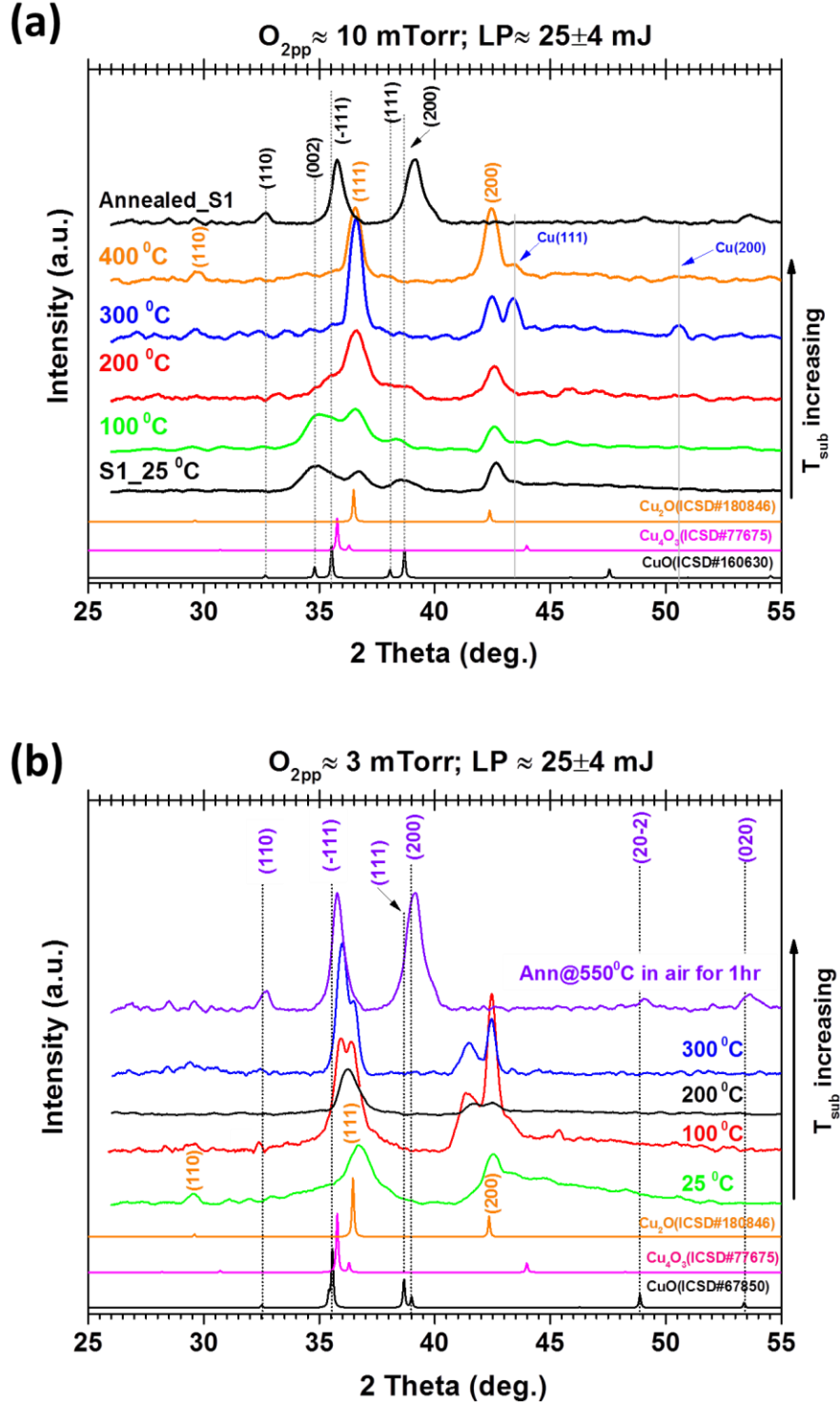


Figure S1 XRD patterns (vertically offset for clarity) of copper oxide thin films deposited onto quartz substrate with a constant laser pulse energy ($LP \approx 25 \pm 4$ mJ) using (a) $O_{2pp} = 10$ mTorr, and $O_{2pp} = 3$ mTorr (b) as a function of substrate temperature. The dotted and solid vertical lines indicate the Bragg reflection peaks of CuO and Cu respectively.

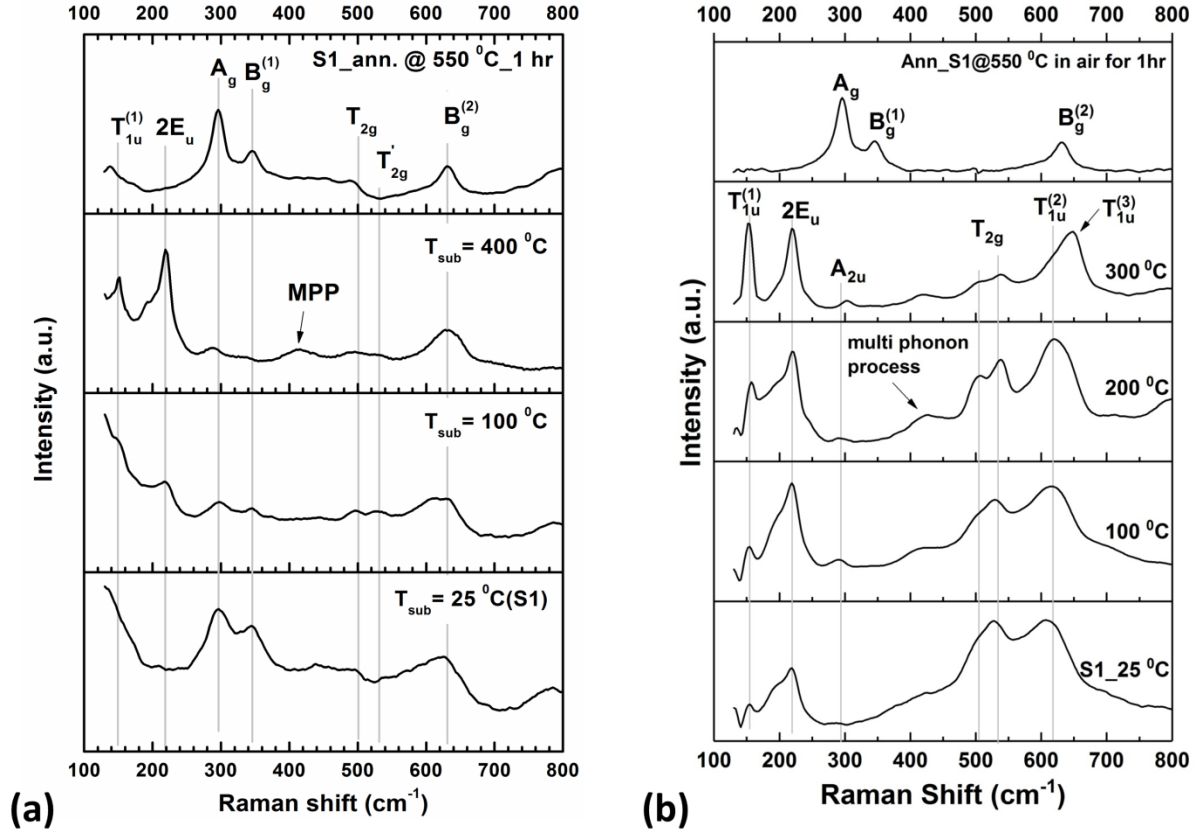


Figure S2 Raman spectra of copper oxide thin films deposited onto quartz substrate with a constant laser pulse energy ($LP \approx 25 \pm 4$ mJ) using (a) $O_{2pp} = 10$ mTorr, and $O_{2pp} = 3$ mTorr (b) as a function of substrate temperature. The vertical lines indicate the reference vibrational modes of copper oxide [1,2].

In order to understand the crystallographic nature of PLD grown Cu_2O films, texture coefficient (figure S3(a)), and crystallite size (figure S3(b)) were analysed as a function of O_{2pp} in both RT- and HT-grown films. Texturing coefficient (f) is calculated from the following formula [2] considering (111) and (200) are the only planes lying parallel to the substrate and hence diffracting strongly:

$$f = 1 - 2y/(x + y) \quad (S1)$$

where, $x = \frac{I(111)}{I(200)}$, $y = \frac{I_0(111)}{I_0(200)}$; $I(hkl)$ and $I_0(hkl)$ are the intensities of (hkl) X-ray reflection planes of as grown thin films and bulk Cu_2O respectively. (XRD of bulk Cu_2O powder scrapped

off from PLD target is shown in figure S7* below). When $f \rightarrow -1$, thin films are highly (200) textured and crystallites are dominantly (111) orientated when $f \rightarrow 1$. One can see that the RT- and HT-grown films approached towards highly {100} and {111} texturing, respectively, with increasing O_{2pp} up to 7 mTorr, appearing to plateau around $O_{2pp} \approx 5$ mTorr which is most probably due to the inclusion of Cu_xO_y species in the Cu_2O matrix.

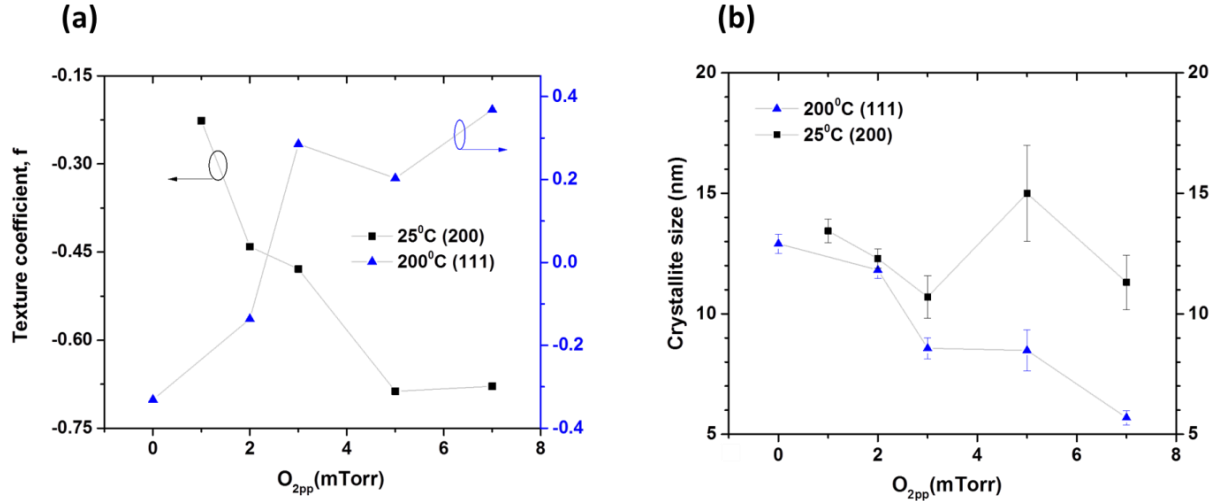


Figure S3. Texture coefficient (a), and average crystallite domain size(b) of Cu_2O films deposited at $T_{sub} \approx 25^\circ C$ (denoted by ■) and $T_{sub} \approx 200^\circ C$ (denoted by ▲) as a function of O_{2pp} .

Figure S3(b) shows the variation of the average crystallites domain size as a function of O_{2pp} . Both for RT- and HT-grown films, grain growth is negatively affected with increasing O_{2pp} ; for example, in case of HT-grown films, crystallite size start to decrease monotonically from ~ 12 nm with no O_{2pp} down to ~ 5 nm with $O_{2pp} \approx 7$ mTorr; suggesting that O_{2pp} must have greater impact on controlling growth rate as well as films microstructure. The likely reason is that higher level of O_{2pp} present during PLD scatter, attenuate and thermalize the ablation plume; consequently lowering the kinetic energy of particle arriving the substrate surface. Therefore, the lower the kinetic energy of adatoms, the slower the grain growth as well as the deposition rate. Furthermore, the crystallite size in HT-grown films are always found to be smaller than those of the RT-grown films irrespective of the O_{2pp} level, indicating that the growth rate in RT-films is faster than HT-films, which, indeed, corroborates the results presented Fig. 6 of the main text.

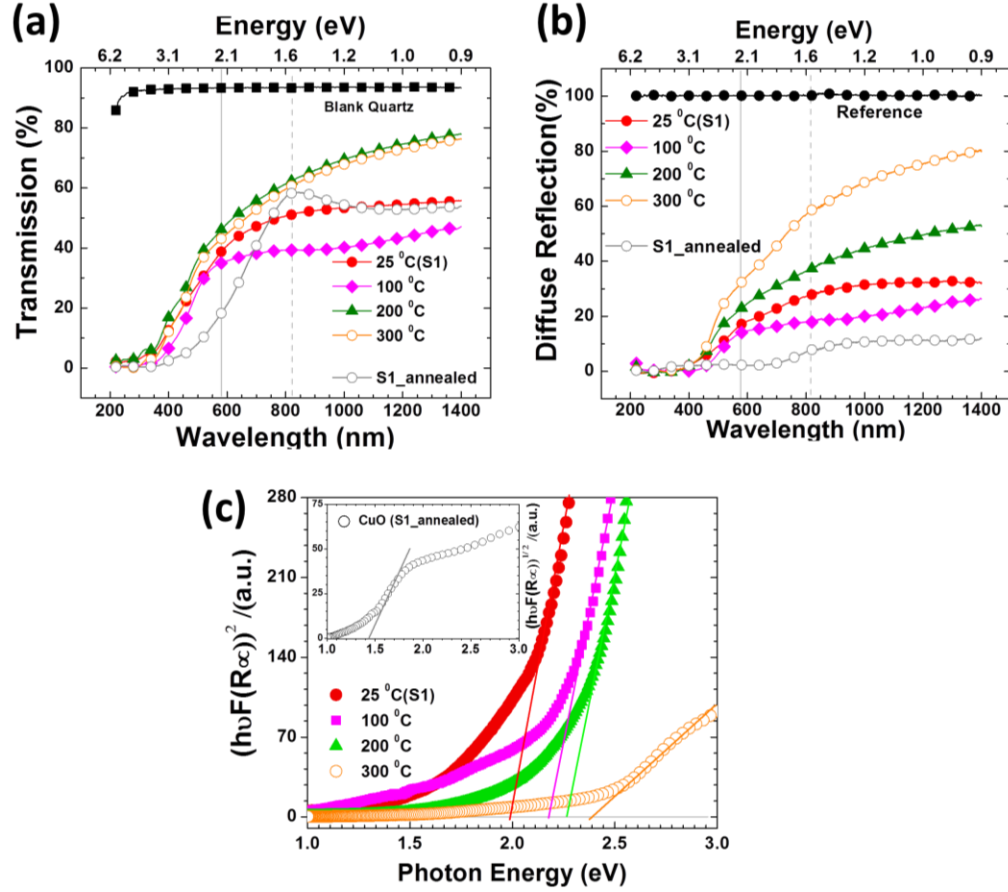


Figure S4 (color online) Transmission (a), diffuse reflection (b) and Tauc plot (c) of PLD grown Cu_2O films as a function of substrate temperature. Tauc plot of the CuO (S1_annealed) film is shown in the inset.

PLD films grown at $\text{O}_{2\text{pp}} = 3 \text{ mTorr}$, $T_{\text{sub}} = 300 \text{ }^\circ\text{C}$ contain predominant Cu_xO_y phase [1] and exhibited a larger bandgap $\sim 2.45 \text{ eV}$ (direct) compared to phase pure Cu_2O film ($E_g = 1.96\text{--}2.20 \text{ eV}$) and RT-grown sample (S1) annealed in air at $550 \text{ }^\circ\text{C}$ for 1 hour exhibited a bandgap $\sim 1.45 \text{ eV}$ (indirect) due to complete conversion to CuO .

The electrical resistivity measured by four point collinear probe exhibited gradual increase in resistivity with increasing substrate temperature at a fixed $\text{O}_{2\text{pp}}$. Figure S5 (below) shows the variation of resistivity (denoted by solid circle (●)) and thickness (denoted by solid rectangle (■)) as a function of T_{sub} at constant $\text{O}_{2\text{pp}} = 3 \text{ mTorr}$. At fixed $\text{O}_{2\text{pp}} = 3 \text{ mTorr}$, the RT($25 \text{ }^\circ\text{C}$)-grown film exhibited ~ 6 order of magnitude lower resistivity ($23 \pm 1 \text{ m}\Omega\cdot\text{cm}$) than those of the films grown at $100 \text{ }^\circ\text{C} \leq T_{\text{sub}} \leq 300 \text{ }^\circ\text{C}$ (their resistivities are found in the range $5 - 30 \text{ k}\Omega\cdot\text{cm}$).

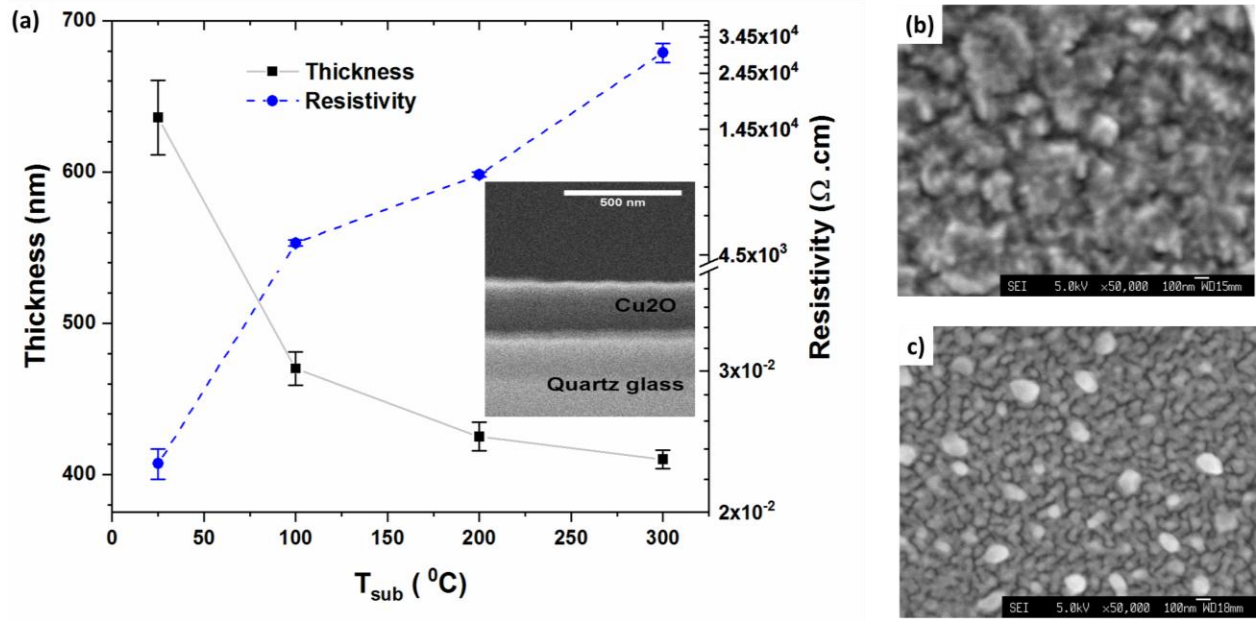


Figure S5 Variation in electrical resistivity and thickness of Cu_2O thin film grown at $\text{O}_{2\text{pp}} = 3$ mTorr as a function of substrate temperature (a); Plane SEM view of Cu_2O film deposited at $T_{\text{sub}} \approx 25^{\circ}\text{C}$ (b) and at $T_{\text{sub}} \approx 300^{\circ}\text{C}$ (c). The thickness data presented in (a) are the average value of VASE and SEM measurements (inset shows a typical cross-sectional SEM view of a sample grown at $T_{\text{sub}} \approx 300^{\circ}\text{C}$).

Notice the film thickness is consistently decreasing from $\sim 635 \pm 25$ nm to $\sim 410 \pm 6$ nm when substrate temperature is elevated from $T_{\text{sub}} = 25^{\circ}\text{C}$ (RT) to $T_{\text{sub}} = 300^{\circ}\text{C}$. (The estimated film thickness of Cu_2O with $2 \text{ mTorr} \leq \text{O}_{2\text{pp}} \leq 7 \text{ mTorr}$ was found to be roughly in the range 550 – 625 nm and 500 – 600 nm for 25°C - and 200°C -grown films respectively). The underlying reason of decreasing film thickness with increasing T_{sub} can be understood as follows: (i) grains/islands are presumably preferred to crystallize with bigger diameter but thinner than the RT-grown grains/islands at elevated T_{sub} due to higher surface mobility of the adatoms; (ii) since surface mobility of adatoms are greater than those of the RT-grown film, therefore, re-sputtering probability from substrate surface held at elevated temperature is high; and (iii) since surface mobility of adatoms are lower at RT-grown film surface therefore they stick together as aggregates on substrate surface and grown faster on vertical direction compared to lateral growth over the period of deposition. Intriguingly, grains in RT-grown film are significantly larger than those of $T_{\text{sub}} \approx 300^{\circ}\text{C}$ -grown film as evident from SEM micrographs (cf. figure S 5(b) and 5(c)), suggesting that the columnar like grain (with a large density of voids) growth in the former and lateral growth in the latter might be playing a vital role in decreasing growth rate with increasing growth temperature. The higher resistivity of thin films grown at elevated T_{sub} suggesting that samples being investigated are in general more oxygen rich as well as stoichiometric compared to RT(25°C)-grown thin films. This observation corroborates the analyses results of XRD

and PL (see figure in the main text).

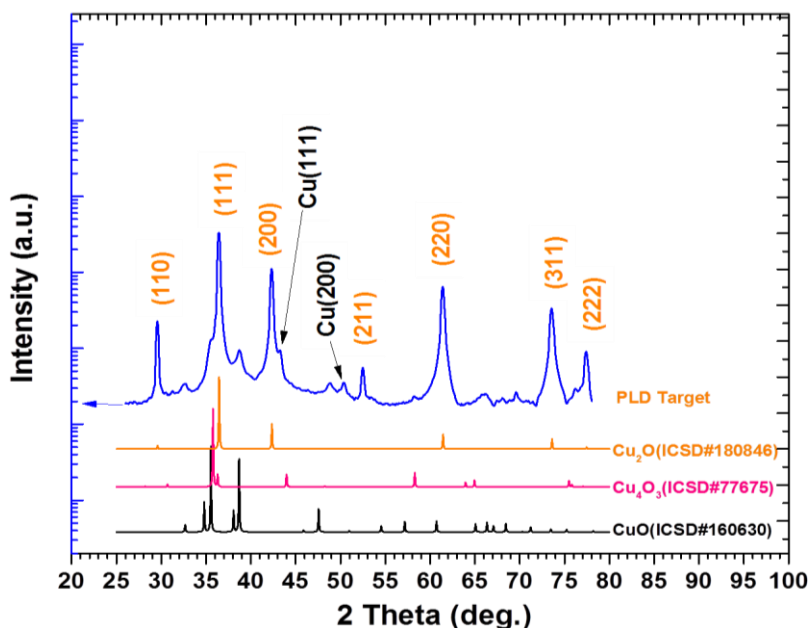


Figure S7* XRD patterns (vertically offset for clarity) of PLD target used for deposition of copper oxide thin films (log scaled indicating by arrow in the left) together with standard ICSD patterns of three different copper-oxide compounds (linear vertical scale in the right)

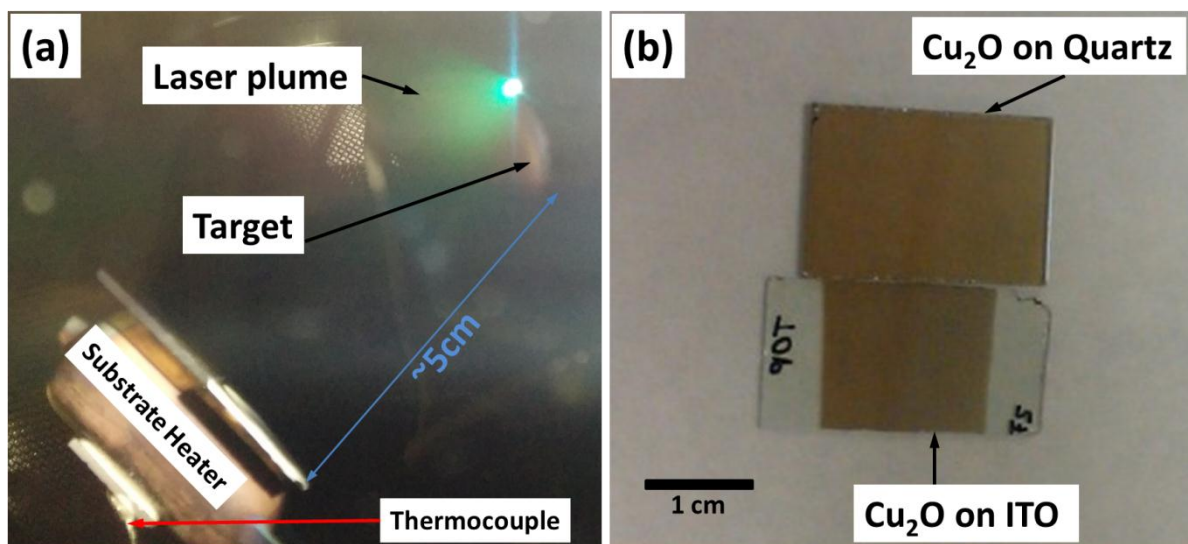


Figure S7 (a) Photograph taken during the synthesis of Cu_2O film on two different substrates in a single deposition session. (b) Photograph of Cu_2O thin films on ITO and Quartz substrate after deposition. Part of ITO was masked with PTFE tape during deposition for selective ohmic contact required for subsequent electrochemical impedance measurements.

Hall mobility measurements:

Hall voltage (also sheet resistance) for couple of samples were carried out in van der Pauw configuration using a standard procedure described in Physical Measurement Laboratory, NIST [3]. Hall voltage measurements were performed using a 1 Tesla permanent magnet and by changing the polarity of, magnetic field (i.e., B(+) and B(-) (manually)) and, sourcing a range of currents (LabVIEW program controlled) in van der Pauw sample configuration (see inset in figure S8(left)). The data analysis procedure can be found in the same reference [3]. All electrical measurements were performed at room temperature under dark.

In commercial Hall effect measurements setup, in general, only one sourcing current has been used for measuring hall voltage, the off-set voltage (see figure S9) due to non-ideal Ohmic contact including asymmetric contact placement, sample shape etc. is often overlooked in final hall voltage measurements as well as hall mobility of the sample being investigated which lead to erroneous results both in conductivity type and mobility. Another issue is to use as minimum source current as possible to avoid joule heating therefore minimize the thermal contribution in the measurement following the ASTM recommendation ref: F46. We considered all issues to estimate the Hall mobility as accurately as possible. Hall voltage (V_H) are measured with varying sourcing current I , an averaged (V_H/I) ratio was used for estimating mobility, $\mu_H = (V_H/I) \times 10^4 \times B^{-1} \times (R_{\square})^{-1}$ where magnetic field B is in Tesla unit, R_{\square} is the sheet resistance in ohm/square. The large offset voltage (Figure S10) seen in the measurements are subtracted to estimate the actual V_H . R_{\square} value measured in 4-point probe was found to be varied ($\pm 2-5\%$) compared to van der Pauw configuration, primarily due to different nature of electrical contact and sample size.

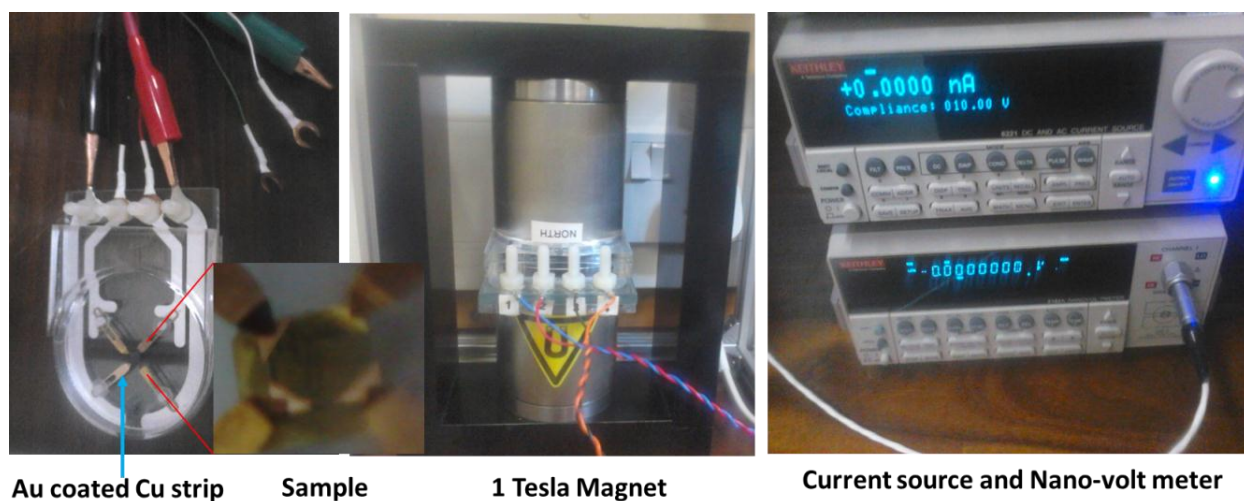


Figure S8 (color online) A precision home-built Hall mobility measurement setup used in this study.

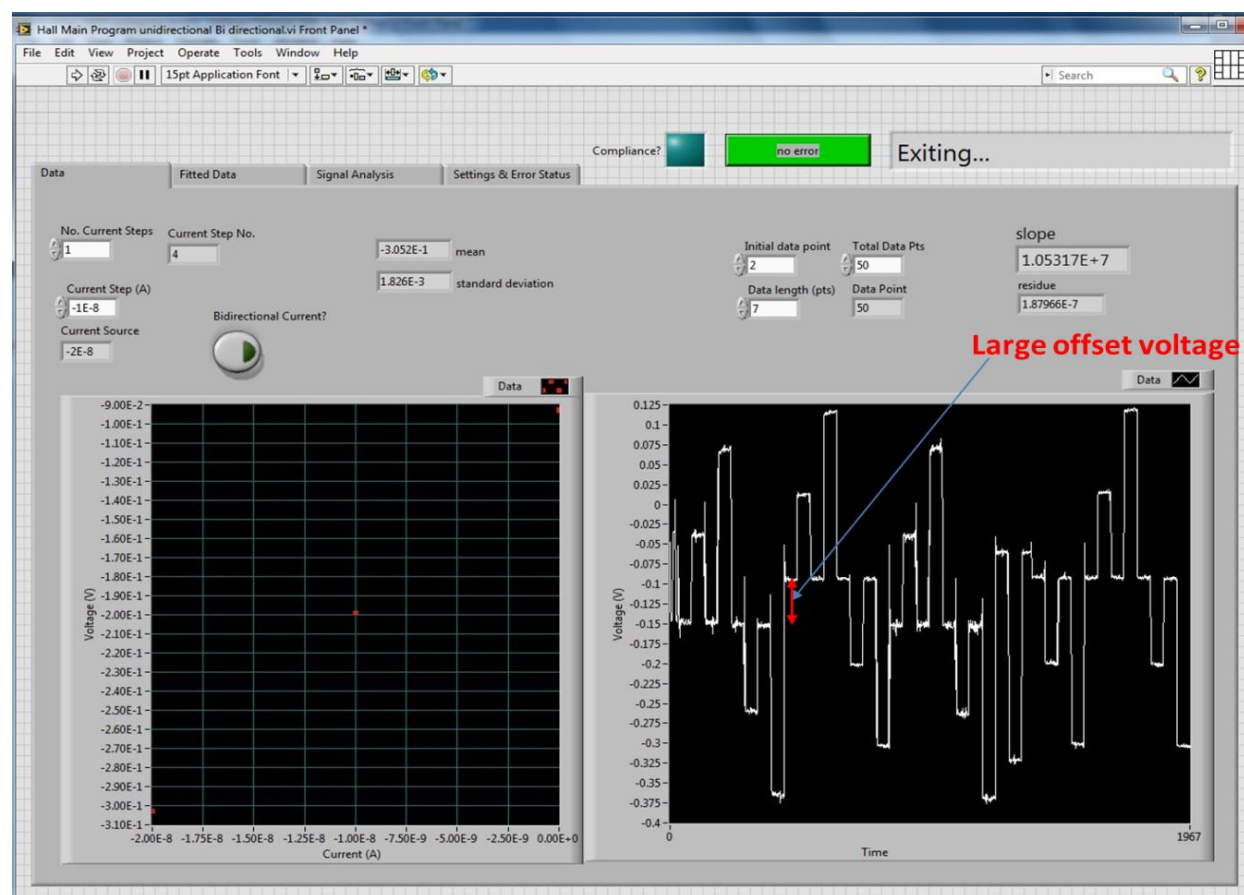


Figure S9 (color online) An example of a large offset voltage (LabVIEW program display) in a typical Hall measurement setup due to non-ideal contact and sample shape.

Electrochemical Impedance Spectroscopy (EIS):

To evaluate electrochemical impedance parameter the Frequency response analyse(FRA) was performed by applying a set of constant bias voltage over a narrow potential window (-0.25 to 0.05 V vs RHE) as mentioned in the experimental section 2, and a standby potential ca. 0.01 V (vs RHE) was maintained after each measurement to avoid possible formation of native CuO atop the film. This was confirmed by doing CV before and after FRA as shown figure S10 evident from the low capacitive current (few μA) within the potential scanning range. It is worth mentioning here that the experimental electrochemical impedance parameters are fitted to a suitable RQ(Q is the constant phase element (CPE) having relation with $C = (Q \cdot R)^{1/n}/R$ and $Q \approx C$ as $n \geq 0.9$) equivalent circuit combination in high frequency region as in figure S11(below) to evaluate true capacitances. Indeed, this capacitance is due to space charge region at the copper oxide|electrolyte interface and capacitances at different bias voltage are used to construct the Mott-Schottky plot shown in Fig. 7(a) in the main text. The Mott-Schottky relation was used to work out V_{fb} and intrinsic carrier density (N_x , where $x = d$ for n-type and a for p-type). The values determined in this way, for desired RT-grown samples, are included in the Table 1(main text) along with other properties as a function of O_{2pp} . The flatband potential converted to vacuum scale using similar method describe in the literature [4] and also depicted in Fig. 7(main text) to identify conduction band(CB) and valence band(VB) with a common reference.

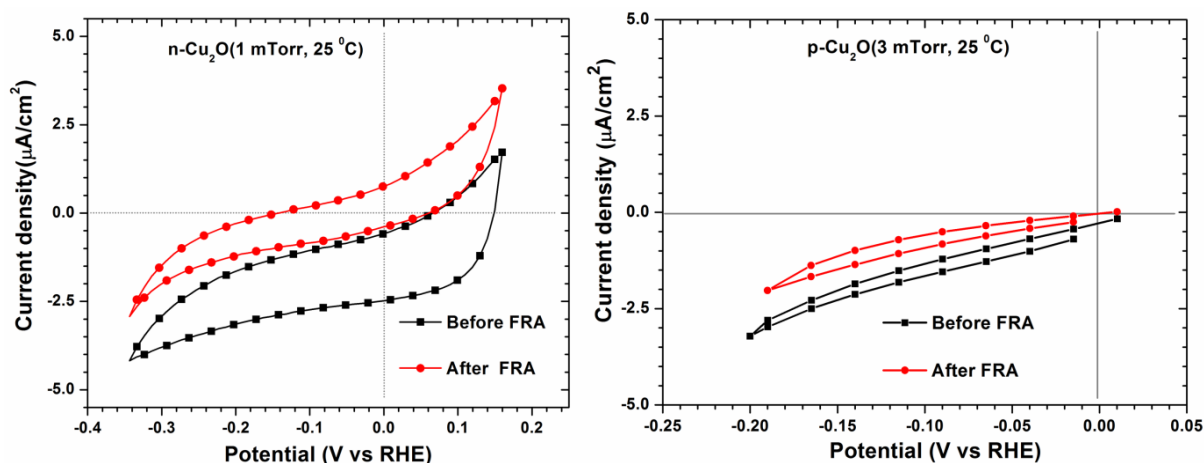


Figure S10 Cyclic voltammograms taken before and after frequency response analyses confirm that there is no-faradic process occurred during EIS measurement.

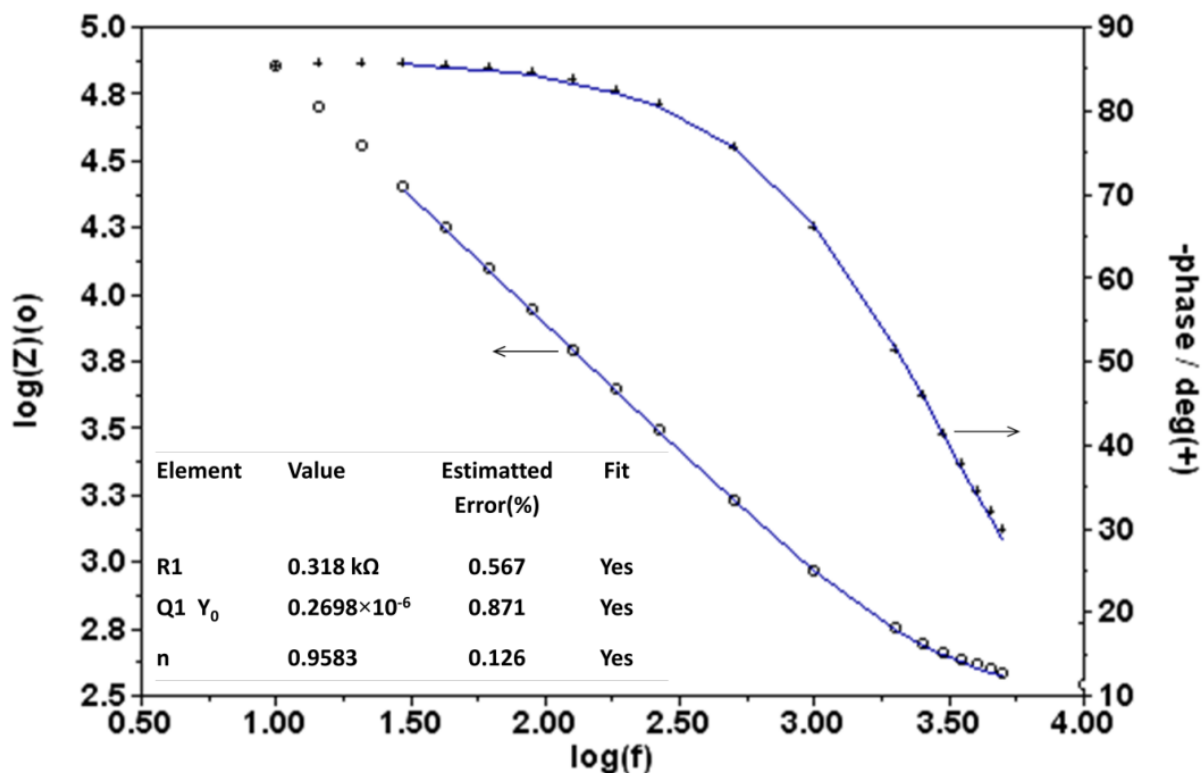


Figure S11 Bode plot of EIS measurements of a RT-grown Cu₂O film on ITO in argon saturated 0.1M CH₃COONa electrolyte at -0.1 V vs RHE, the solid line represent the fits using an RQ equivalent(Q≈ C as n≥0.9). First few data points are eliminated to minimize the error in the best fitted impedance parameters(see inset table).

Calculation of effective density of states ($D(E_f)$) from EIS data:

The total double-layer capacitance(C_T) of copper oxide|electrolyte system can be calculated from the imaginary impedance(Z_{imag}) using equation [5]:

$$C_T = -1/(2\pi f Z_{imag}) \quad (S2)$$

where, f is the frequency. The space charge capacitance(C_{sc}) and Helmholtz capacitance (C_H)[6] can be related to C_T by following equation:

$$1/C_T = 1/C_{sc} + 1/C_H \quad (S3)$$

For, Cu₂O/ITO electrode grown at 25 °C with O₂pp = 3 mTorr, using equation (S2) we got, C_T = 11.25 μF/cm² (where, f = 29.76 Hz and -Z_{imag} ≈ 6790 Ohm) at -0.21 V vs Ag/AgCl(≈0 V vs RHE) considering similar approach described in ref.[5].

Assuming C_H >> C_{sc} ; C_{sc} ≈ C_T ≈ 11.25 × 10⁻² F/m²

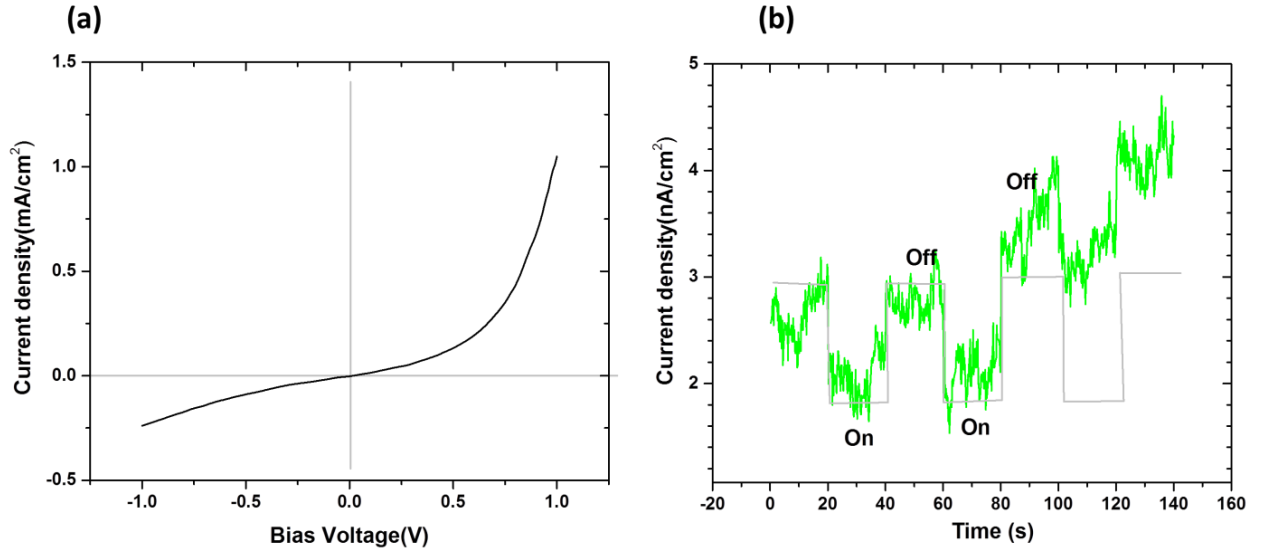
Therefore, the effective density states, $D(E_f) = (C_{sc})^2 / [\epsilon_0 \epsilon \cdot e^2] \approx 1.35 \times 10^{21} \text{ cm}^{-3}/(\text{eV})$.

[Or, incase of highly doped electrodes, assuming C_H = 20 μF/cm²[5] equation(S3) yields, C_{sc} ≈ 25.70 μF/cm²; $D(E_f) \approx 7.06 \times 10^{21} \text{ cm}^{-3}/(\text{eV})$]

where, ε₀ is permittivity of free space (8.854 × 10⁻¹² F.m⁻¹), ε is the relative dielectric constant(≈6.6 for Cu₂O [7]) and e is the electronic charge ~1.60 × 10¹⁹ C.

Similarly, we estimated effective density of states for other samples.

Fabrication of solid p-n junctions using p- and n-type Cu₂O:



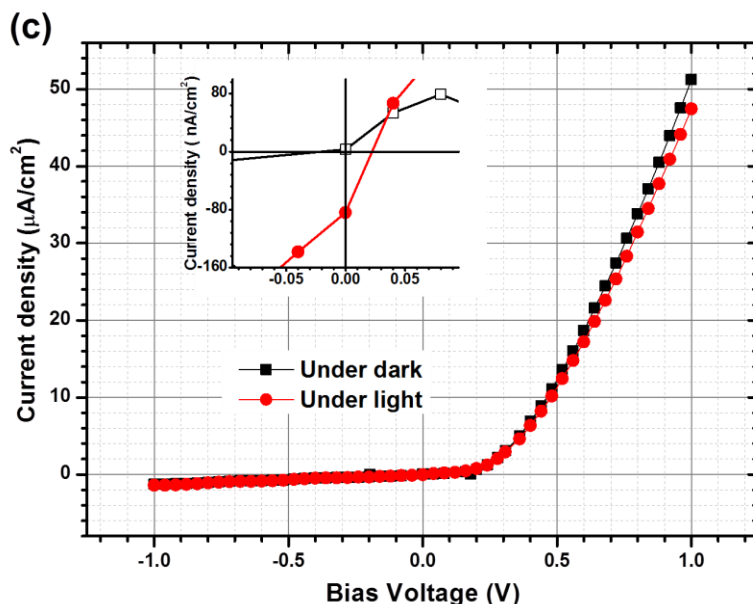


Figure S12. The characteristic J-V curve for n-ZnO/p-Cu₂O (a, b) and n-Cu₂O/p-Si(111)(c) solar cells. Transient photocurrent of n-ZnO/p-Cu₂O cell measured under periodic LED illumination where ‘On’ and ‘Off’ step of the transient photocurrent (b) is demonstrated by the faint curve to assist the reader. A zoomed J-V curve under dark and light is shown in the inset of (c).

In figure S12(a), the dark J-V characteristics curve of FTO/n-ZnO/p-Cu₂O/Au (cell#1) cell exhibited stable rectifying behaviour suggesting that a p-n junction was formed in the Cu₂O-ZnO system. If p-n junction did not form, the dark and illuminated J-V curve would exhibit an ohmic behaviour and change the resistance of the system. The presence of high reverse saturation current of this cell is chiefly due to poor quality p-n junction (see Figure S13 below). The downward shift of illuminated J-V curve was not consistent all time, therefore, taking an illuminated J-V curve within the narrow scanning range (e.g., -0.002 to +0.002V) would not produce reliable short circuit current (J_{sc}) and open circuit voltage (V_{oc}). However, the dynamic photo response at zero bias voltage of the same cell switching with the LED (wavelength just above the band gap of the absorber Cu₂O ($E_g \approx 2.2\text{eV}$ (564nm)) layer) by a pulse width of 20 sec exhibited very low and noisy photocurrent yet distinguishable from the dark current (see figure S12(b)). The synchronized ‘on’ and ‘off’ photo response of the cell#1 with the LED switching confirms that J_{sc} ($\sim 1\text{ nA/cm}^2$) is real despite the noise fluctuation (see faint and green curve in figure S12(b)). Therefore, very low J_{sc} of the PV cell#1 could be attributed to low numbers of

photogenerated charge carriers owing to ‘thin and poor quality’ Cu₂O layer (~53 nm) and thin ZnO(~114nm) layer including an amorphous interfacial layer evident from the subsequent focused ion beam (FIB) cross-section and TEM analyses (see Figure S13 below). Referring to figure S12 (b), the dark current density is increasing over time but the amplitude of the J_{sc} is remaining roughly the same on average (J_{sc} ~1 nA/cm²). The increase of dark current over time and low photocurrent might be attributed to the poor quality Cu₂O/ZnO junction owing to the presence of interfacial states which can serve as a recombination centre for the photogenerated charge carriers.

Figure 8(c) shows the J-V characteristics curve of p-Si(111)/n-Cu₂O (cell#2) under dark and light (The I-V curve for ohmic contact for this cell can be found in Figure S14). A zoomed part of this J-V curve is included in the inset of (c) to distinguish low J_{sc} ~ 80 nA/cm² and V_{oc} ~3 mV. Though a feeble PV performance, the J_{sc} and V_{oc} of cell#2 composed of PLD grown n-type Cu₂O on commercial p-Si substrate clearly better than cell#1. The interfacial investigation of cell#2 by FIB-TEM techniques was not done in this study which would give valuable information for further PV performance improvement.

Interface of n-ZnO/p-Cu₂O (cell#1):

To investigate the interface between ZnO and Cu₂O layer, a cross-section of the n-ZnO/p-Cu₂O(cell#1) cell was made by focused ion beam (FIB) technique. The SEM micrograph of the FIB specimen confirmed the formation of very thin but continuous Cu₂O (~53nm) and ZnO (~114nm) layer across the specimen (see figure S12 (top panel) overleaf). However, the subsequent TEM bright field (BF) image of the FIB specimen revealed an amorphous layer between the Cu₂O and ZnO layer (see figure S12 (bottom panel #4 inset) overleaf). It was expected that 30 minute deposition time would give ~300 nm thick Cu₂O films, but both SEM and TEM BF image revealed a thickness which is much lower than the expected thickness. One possible reason might be the ZnO coating of quartz window occurred during ZnO film deposition step. Therefore, most of the UV-radiation might be absorbed or/and allow less amount (and less energetic) of radiation to fall on the Cu₂O target. This should affect the quantity of ablated species from the target as well as subsequent Cu₂O formation on the substrate. This means that one could expect a thin and poor quality Cu₂O film on any substrate, which resulted in poor quality interface between the deposited film and the substrate. A good quality Cu₂O film having

absorption cross-section $\sim 10^5 \text{ cm}^{-1}$ near the band edge suggest that at least $\sim 100 \text{ nm}$ thick layer is necessary for sufficient numbers of photons to be absorbed (Thicker layer is also desired to avoid short-circuiting between inter layers). Therefore, very low J_{sc} of the present PV cell could be attributed to low numbers of photogenerated charge carriers owing to ‘thin and poor quality’ Cu_2O layer.

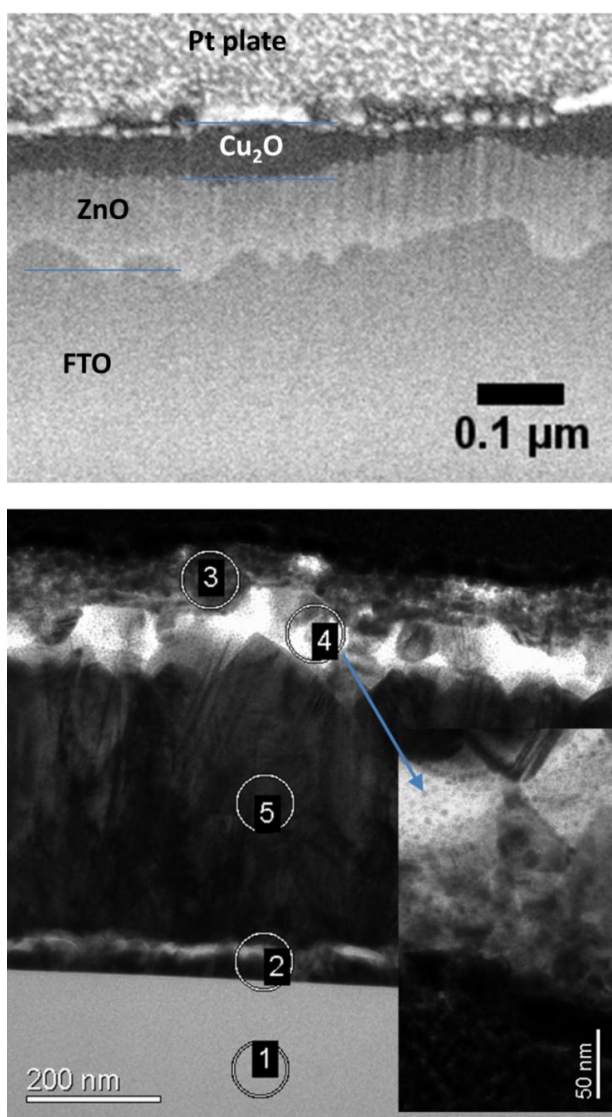


Figure S13 FIB cross section of $\text{ZnO}/\text{Cu}_2\text{O}$ solar cell junction (top): Cu_2O ($\sim 53 \text{ nm}$), and ZnO ($\sim 114 \text{ nm}$) layer. TEM Bright field image of the FIB cross-sectional sample (bottom left). Bottom left: Cu_2O (#3); amorphous layer (#4) between ZnO and Cu_2O layer (Shown bottom inset); FTO (#5 & #2) SiO_2 (#2) and Glass (#1). Platinum (Pt)-plate was used to protect thin layers during FIB cross-sectional specimen preparation.

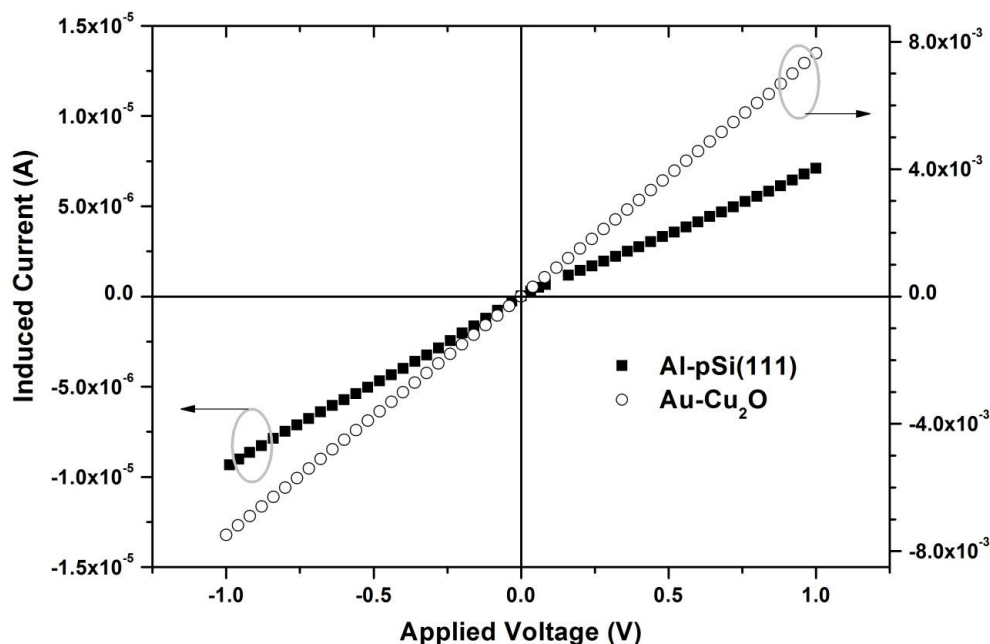


Figure S14 I-V curve of p-Si (solid square) and n-Cu₂O (open circle) with aluminium and gold contacts showing ohmic behaviour.

References

- [1] S.F.U. Farhad, R.F. Webster, D. Cherns, Electron microscopy and diffraction studies of pulsed laser deposited cuprous oxide thin films grown at low substrate temperatures, *Materialia*, 3 (2018) 230 - 238.
- [2] S.F.U. Farhad, Copper Oxide Thin Films grown by Pulsed Laser Deposition for Photovoltaic Applications, in: School of Physics, University of Bristol, UK, 2016, pp. 222.
- [3] Van der Pauw Hall Measurement worksheet, Physical Measurement Laboratory, National Institute of Standards and Technology (NIST). Accessed on 22/12/2014, in, NIST, NIST website.
- [4] C.M. McShane, K.S. Choi, Junction studies on electrochemically fabricated p-n Cu₂O homojunction solar cells for efficiency enhancement, *Physical chemistry chemical physics : PCCP*, 14 (2012) 6112-6118.
- [5] B. Bera, A. Chakraborty, T. Kar, P. Leuaa, M. Neergat, Density of States, Carrier Concentration, and Flat Band Potential Derived from Electrochemical Impedance Measurements of N-Doped Carbon and Their Influence on Electrocatalysis of Oxygen Reduction Reaction, *The Journal of Physical Chemistry C*, 121 (2017) 20850-20856.
- [6] K. Uosaki, Effects of the Helmholtz Layer Capacitance on the Potential Distribution at semiconductor/Electrolyte Interface and the Linearity of the Mott-Schottky Plot, *Journal of The Electrochemical Society*, 130 (1983) 895.
- [7] A. Paracchino, J.C. Brauer, J.-E. Moser, E. Thimsen, M. Graetzel, Synthesis and Characterization of High-Photoactivity Electrodeposited Cu₂O Solar Absorber by Photoelectrochemistry and Ultrafast Spectroscopy, *The Journal of Physical Chemistry C*, 116 (2012) 7341-7350.